nature ecology & evolution

ARTICLES

https://doi.org/10.1038/s41559-022-01801-3

Check for updates

Prolonged morphological expansion of spiny-rayed fishes following the end-Cretaceous

Ava Ghezelayagh[1,18]✉, Richard C. Harrington[1,18]✉, Edward D. Burress[1], Matthew A. Campbell[2,3], Janet C. Buckner[4,5], Prosanta Chakrabarty[6], Jessica R. Glass[7], W. Tyler McCraney[5], Peter J. Unmack[8], Christine E. Thacker[9,10], Michael E. Alfaro[5], Sarah T. Friedman[1,11], William B. Ludt[10], Peter F. Cowman[12], Matt Friedman[13,14], Samantha A. Price[15], Alex Dornburg[16], Brant C. Faircloth[6], Peter C. Wainwright[11] and Thomas J. Near[1,17]

Spiny-rayed fishes (Acanthomorpha) dominate modern marine habitats and account for more than a quarter of all living vertebrate species. Previous time-calibrated phylogenies and patterns from the fossil record explain this dominance by correlating the origin of major acanthomorph lineages with the Cretaceous–Palaeogene mass extinction. Here we infer a time-calibrated phylogeny using ultraconserved elements that samples 91.4% of all acanthomorph families and investigate patterns of body shape disparity. Our results show that acanthomorph lineages steadily accumulated throughout the Cenozoic and underwent a significant expansion of among-clade morphological disparity several million years after the end-Cretaceous. These acanthomorph lineages radiated into and diversified within distinct regions of morphospace that characterize iconic lineages, including fast-swimming open-ocean predators, laterally compressed reef fishes, bottom-dwelling flatfishes, seahorses and pufferfishes. The evolutionary success of spiny-rayed fishes is the culmination of multiple species-rich and phenotypically disparate lineages independently diversifying across the globe under a wide range of ecological conditions.

Spiny-rayed fishes (Acanthomorpha) account for more than a quarter of all living vertebrates and are globally distributed across all types of aquatic ecosystem[1–4]. Acanthomorphs are especially prevalent in modern nearshore marine habitats, with familiar representatives including sticklebacks, seahorses and commercially important species such as cod, tuna and flatfishes. Despite the scientific, economic and cultural importance of acanthomorphs, how spiny-rayed fishes diversified to become the dominant marine vertebrate lineage remains relatively unexplored.

The evolutionary success of acanthomorph fishes has repeatedly been linked to the Cretaceous–Palaeogene (K–Pg) mass extinction[3,5–7], which occurred 66 million years ago (Ma) and is understood to have laid the foundation for spectacular radiations of terrestrial vertebrates[8–15]. The most inclusive lineages of acanthomorph fishes (for example, Syngnathiformes, Labriformes and Perciformes) originated before or during the Late Cretaceous[3,16,17], but Palaeogene fossils demonstrate that acanthomorph taxonomic diversity and morphological disparity increased substantially after the K–Pg event[6]. Phylogenomic analyses have raised the complementary proposal that the origins of many major acanthomorph lineages coincide with the K–Pg[7,18]. However, the acanthomorph fossil record is sparse in the 20 million years around the end-Cretaceous[6,16], and phylogenomic efforts so far have been limited by sampling designs that inadequately represent the group's staggering taxonomic richness[7,18]. These factors have hindered resolution of the timing and patterns of acanthomorph diversification near the K–Pg; it remains uncertain if acanthomorph diversification in the Cenozoic was gradual or punctuated, whether lineage diversification is coupled with phenotypic disparity, and how individual lineages contributed to a collective pattern of acanthomorph diversification. A well-resolved, time-calibrated phylogeny that includes all major lineages is critical to understanding the evolutionary dynamics of spiny-rayed fishes across the K–Pg boundary and beyond.

The largest challenge to acanthomorph evolutionary studies is inferring a phylogeny of its more than 19,450 species[1,4]. The resolution of relationships within the subclade Percomorpha, which contains more than 95% of all acanthomorph species, has been particularly difficult. During most of the twentieth century, inferences of acanthomorph and percomorph relationships relied on anatomical characters that resulted in largely unresolved phylogenetic hypotheses[19]. Although these early morphological investigations defined major groups of acanthomorphs, their conclusions were dramatically upended by the introduction of phylogenies inferred from a relatively small number of Sanger-sequenced

[1]Department of Ecology and Evolutionary Biology, Yale University, New Haven, CT, USA. [2]Department of Animal Science, University of California, Davis, CA, USA. [3]University of Alaska Museum of the North, Fairbanks, AK, USA. [4]Department of Biology, University of Texas, Arlington, TX, USA. [5]Department of Ecology and Evolutionary Biology, University of California, Los Angeles, CA, USA. [6]Museum of Natural Science and Department of Biological Sciences, Louisiana State University, Baton Rouge, LA, USA. [7]College of Fisheries and Ocean Sciences, University of Alaska Fairbanks, Fairbanks, AK, USA. [8]Institute for Applied Ecology, University of Canberra, Canberra, Australian Capital Territory, Australia. [9]Santa Barbara Museum of Natural History, Santa Barbara, CA, USA. [10]Natural History Museum of Los Angeles County, Los Angeles, CA, USA. [11]Department of Evolution and Ecology, University of California, Davis, CA, USA. [12]Queensland Museum, Townsville, Queensland, Australia. [13]Department of Earth and Environmental Sciences, University of Michigan, Ann Arbor, MI, USA. [14]Museum of Paleontology, University of Michigan, Ann Arbor, MI, USA. [15]Department of Biological Sciences, Clemson University, Clemson, SC, USA. [16]Department of Bioinformatics and Genomics, University of North Carolina, Charlotte, NC, USA. [17]Peabody Museum of Natural History, Yale University, New Haven, CT, USA. [18]These authors contributed equally: Ava Ghezelayagh, Richard C. Harrington. ✉e-mail: ava.ghezelayagh@gmail.com; richard.harrington@yale.edu

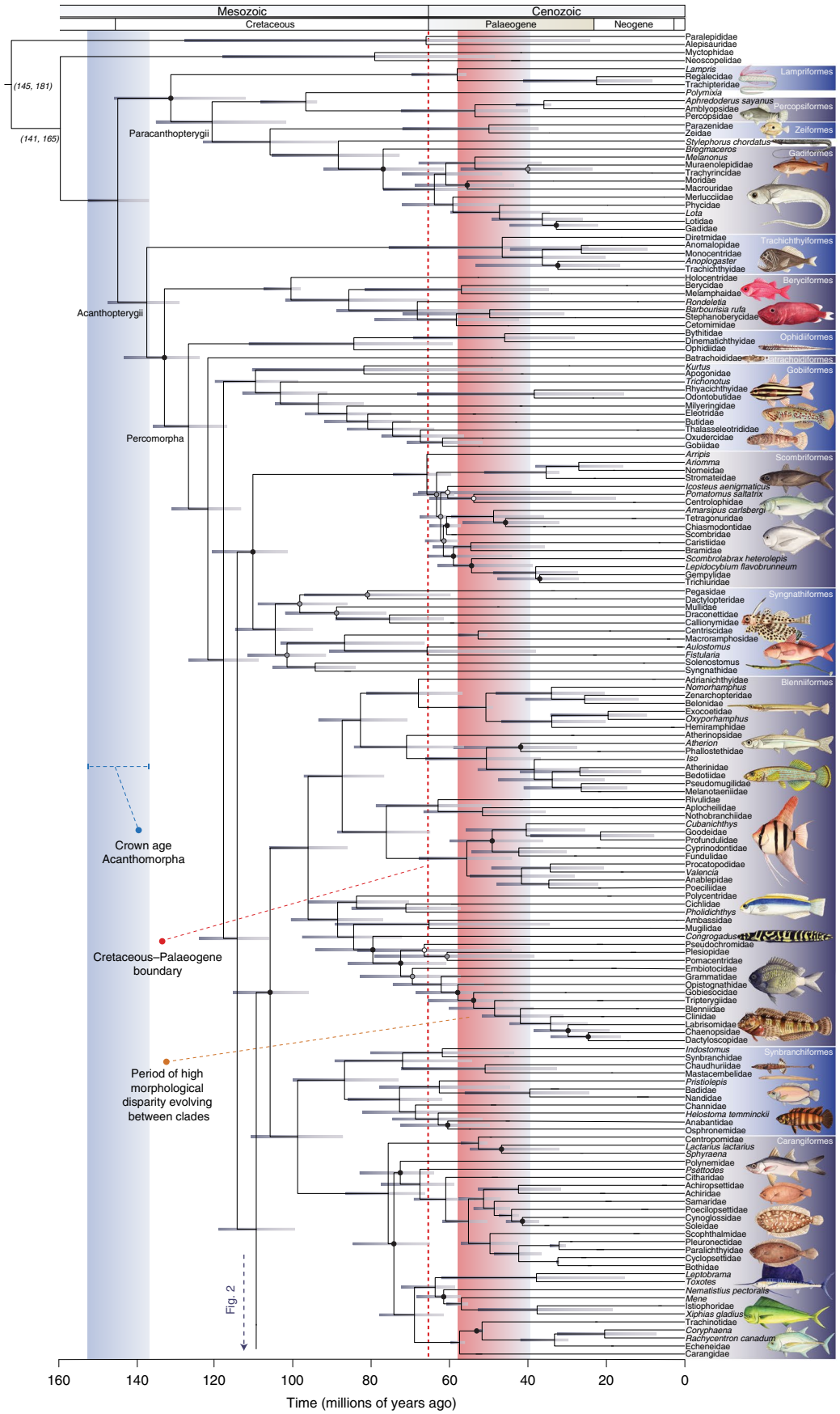
Mesozoic
Cenozoic
Cretaceous
Palaeogene
Neogene
(145, 181)
(141, 165)
Paracanthopterygii
Acanthopterygii
Percomorpha
Crown age Acanthomorpha
Cretaceous–Palaeogene boundary
Period of high morphological disparity evolving between clades
Fig. 2
Paralepididae
Alepisauridae
Myctophidae
Neoscopelidae
Lampris
Regalecidae
Trachipteridae
Polymixia
Aphredoderus sayanus
Amblyopsidae
Percopsidae
Parazenidae
Zeidae
Stylephorus chordatus
Bregmaceros
Melanonus
Muraenolepididae
Trachyrincidae
Moridae
Macrouridae
Merluccidae
Phycidae
Lota
Lotidae
Gadidae
Diretmidae
Anomalopidae
Monocentridae
Anoplogaster
Trachichthyidae
Holocentridae
Berycidae
Melamphaidae
Rondeletia
Barbourisia rufa
Stephanoberycidae
Cetomimidae
Bythitidae
Dinematichthyidae
Ophidiidae
Batrachoididae
Kurtus
Apogonidae
Trichonotus
Rhyacichthyidae
Odontobutidae
Milyeringidae
Eleotridae
Butidae
Thalasseleotrididae
Oxudercidae
Gobiidae
Arripis
Aniomma
Nomeidae
Stromateidae
Icosteus aenigmaticus
Pomatomus saltatrix
Centrolophidae
Amarsipus carlsbergi
Tetragonuridae
Chiasmodontidae
Scombridae
Caristiidae
Bramidae
Scombrolabrax heterolepis
Lepidocybium flavobrunneum
Gempylidae
Trichiuridae
Pegasidae
Dactylopteridae
Mullidae
Draconettidae
Callionymidae
Centriscidae
Macroramphosidae
Aulostomus
Fistularia
Solenostomus
Syngnathidae
Adrianichthyidae
Nomorhamphus
Zenarchopteridae
Belonidae
Exocoetidae
Oxyporhamphus
Hemiramphidae
Atherinopsidae
Atherion
Phallostethidae
Iso
Atherinidae
Bedotiidae
Pseudomugilidae
Melanotaeniidae
Rivulidae
Aplocheilidae
Nothobranchiidae
Cubanichthys
Goodeidae
Profundulidae
Cyprinodontidae
Fundulidae
Procatopodidae
Valencia
Anablepidae
Poeciliidae
Polycentridae
Cichlidae
Pholidichthys
Ambassidae
Mugilidae
Congrogadus
Pseudochromidae
Plesiopidae
Pomacentridae
Embiotocidae
Grammatidae
Opistognathidae
Gobiesocidae
Tripterygiidae
Blenniidae
Clinidae
Labrisomidae
Chaenopsidae
Dactyloscopidae
Indostomus
Synbranchidae
Chaudhuriidae
Mastacembelidae
Pristiolepis
Badidae
Nandidae
Channidae
Helostoma temminckii
Anabantidae
Osphronemidae
Centropomidae
Lactarius lactarius
Sphyraena
Polynemidae
Psettodes
Citharidae
Achiropsettidae
Achiridae
Samaridae
Poecilopsettidae
Cynoglossidae
Soleidae
Scophthalmidae
Pleuronectidae
Paralichthyidae
Cyclopsettidae
Bothidae
Leptobrama
Toxotes
Nematistius pectoralis
Mene
Istiophoridae
Xiphias gladius
Trachinotidae
Coryphaena
Rachycentron canadum
Echeneidae
Carangidae
Lampriformes
Percopsiformes
Zeiformes
Gadiformes
Trachichthyiformes
Beryciformes
Ophidiiformes
Batrachoidiformes
Gobiiformes
Scombriformes
Syngnathiformes
Blenniiformes
Synbranchiformes
Carangiformes
160
140
120
100
80
60
40
20
0
Time (millions of years ago)

Fig. 1 | Time-calibrated phylogeny of Acanthomorpha, continued in Fig. 2. The phylogeny is condensed to represent taxonomic families at the tips. Monotypic families are represented by the species or genus name. Shaded tabs to the right of taxon labels identify inclusive taxonomic orders. Maximum likelihood bootstrap support (BSS) values for relationships are in Supplementary Figs. 1–15, but unmarked nodes have 100% BSS and nodes with BSS values <97% are indicated by light-grey circles. Nodes with black circles indicate subtending branches with sCF values lower than one or two site discordance (sDF) values, while nodes with dark-grey circles indicate lower sCF values and BSS values <97%. Horizontal grey bars at each node portray the 95% highest posterior density (HPD) credible interval of node age estimates. The blue shaded region reflects the 95% HPD credible interval of the crown age of Acanthomorpha. A vertical red dashed line marks the K–Pg. The red shaded region corresponds to the disparity through time plot in Fig. 2 and reflects a period of heightened among-clade morphological disparity in Acanthomorpha. Fish illustrations by Julie Johnson.

mitochondrial and nuclear genes[3,17,20–22]. For instance, molecular phylogenies resolved the anglerfishes—long classified with the group of non-percomorph acanthomorphs that includes the economically important cods (Gadiformes)—well within Percomorpha as the sister lineage of the pufferfishes and their allies[3,17,21]. In addition, molecular phylogenies have identified several major lineages of percomorphs that each encompass a large number of species and taxonomic families[3,4,17]. As an example, one of these lineages discovered in molecular phylogenetic studies contains such ecologically and phenotypically disparate lineages as cichlids, blennies, guppies, flyingfishes, surfperches and mullets[22]. Despite this progress, the inter-relationships among and within the major lineages of percomorphs and acanthomorphs remain unresolved owing to limited informativeness in Sanger DNA sequence datasets and limited taxonomic sampling of previous phylogenomic analyses[3,7,17,18,21–23].

In this Article, we present the results of comprehensive phylogenomic analyses and estimates of divergence times for 1,084 species representing 308 of the 337 (91.4%) acanthomorph taxonomic families (Supplementary Table 1). We sampled nine species from Aulopiformes (lizardfishes), Myctophidae (lanternfishes) and Neoscopelidae (blackchins) to serve as outgroups. Our phylogenomic inferences are based on a DNA sequence alignment of 989 ultraconserved element (UCE) loci, and our divergence time estimates were calibrated with 43 fossil constraints. We combine this new acanthomorph time tree with phenotypic data for 680 living acanthomorph species[24] to explore the evolutionary patterns of body shape disparity in spiny-rayed fishes.

Results and discussion

The results of the maximum likelihood analysis of the concatenated UCE dataset depart from previous efforts by yielding confident phylogenetic resolution of nearly all sampled families of acanthomorphs and percomorphs (Figs. 1 and 2 and Supplementary Figs. 1–25). The UCE phylogeny differs from a phylogenomic analysis of exon capture data[18] in the identification of Paracanthopterygii as monophyletic and sister to Lampriformes, the resolution of a clade containing beardfishes (*Polymixia*) and Percopsiformes (trout-perches, pirate perch and amblyopsid cavefishes), and the placement of Beryciformes (containing Berycoidei and Holocentridae) as the sister lineage of the species-rich Percomorpha, each supported by high bootstrap values and estimates of Bayesian concordance factors (Figs. 1 and 3). The phylogenies resulting from analyses of these concatenated exon markers also support the common ancestry of Beryciformes and Percomorpha, and the deepest nodes within Paracanthopterygii are poorly supported[18]. Our results are consistent with earlier molecular analyses in regard to the resolution of major percomorph clades that each include a large number of taxonomic families[3,7,17,18,21]. For example, our analyses resolve the percomorph subclade Acanthuriformes[4,25] as a monophyletic group comprising more than 2,325 species that includes anglerfishes, pufferfishes, butterflyfishes and scores of other percomorph lineages that have long evaded resolution in morphological and molecular analyses (Fig. 2).

In addition to resolving major lineages and taxonomic families, the maximum likelihood UCE phylogeny reveals novel relationships among some of the most scientifically interesting lineages of percomorph fishes (Figs. 1 and 2 and Supplementary Figs. 1–25). For example, Sanger sequencing studies led to the discovery that the enigmatic coral reef-dwelling engineer gobies (*Pholidichthys*) are the sister lineage of cichlids[3,17,22] (Fig. 1 and Supplementary Fig. 11). Whereas these Sanger analyses offered weak resolution beyond the monophyly of these two lineages, our maximum likelihood UCE phylogeny resolves the freshwater tropical African and South American leaffishes (Polycentridae) as the sister lineage of the *Pholidichthys*–cichlid clade, providing an opportunity for insight into the evolution of the remarkable species richness and key morphological novelties found in cichlid fishes. We also confidently resolve the nearshore rocky reef-dwelling false scorpionfish (*Centrogenys vaigiensis*) as the sister lineage to a clade of more than 630 species of wrasses and parrotfishes (Labridae) (Fig. 2 and Supplementary Fig. 21). Consistent with this discovery is that wrasses and *Centrogenys vaigiensis* share ancestral, highly modified components of the 'labroid' pharyngeal jaw apparatus[22]. This result thereby reduces the number of inferred independent evolutions of pharyngognathy, an advanced feeding mechanism that promotes trophic diversification by freeing the oral jaws from prey-processing functions[22,26].

Maximum likelihood concordance factor analyses using single-locus trees allow for a closer examination of node support and potential sources of discordance in the acanthomorph phylogeny. Phylogenetic inference on large, concatenated datasets of short sequences such as UCE loci are known to inflate nodal bootstrap support values[27,28]. It is prudent to interpret high bootstrap support for difficult-to-resolve nodes or those supporting the resolution of contentious phylogenetic relationships with caution, distinguishing between the sampling variance that determines bootstrap support and the observed variance in the original data. We measure this underlying variation using site- and gene-concordance factors

Fig. 2 | Time-calibrated phylogeny and subclade disparity through time for Acanthomorpha, continued from Fig. 1. Continuation of the time-calibrated phylogeny condensed to represent taxonomic families at the tips. Shaded tabs to the right of taxon labels identify inclusive taxonomic orders. Maximum likelihood bootstrap support (BSS) values for relationships are in Supplementary Figs. 16–25, but unmarked nodes have 100% BSS and nodes with BSS values <97% are indicated by light-grey circles. Nodes with black circles indicate subtending branches with sCF values lower than one or two site discordance (sDF) values, while nodes with dark-grey circles indicate lower sCF values and BSS values <97%. Horizontal grey bars at each node portray the 95% highest posterior density (HPD) credible interval of node age estimates. The blue shaded region reflects the 95% HPD credible interval of the crown age of Acanthomorpha. A vertical red dashed line marks the K–Pg. The solid blue line shows observed average relative morphological disparity through time (DTT) for all of Acanthomorpha (represented in both Figs. 1 and 2), and the orange portion of the line, which corresponds to the vertical red shading, reflects the high among-clade disparity present in the early Eocene. The dashed black line and surrounding grey envelope represent the mean DTT and 95% confidence interval for Acanthomorpha as predicted under Brownian evolution, respectively. Fish illustrations by Julie Johnson.

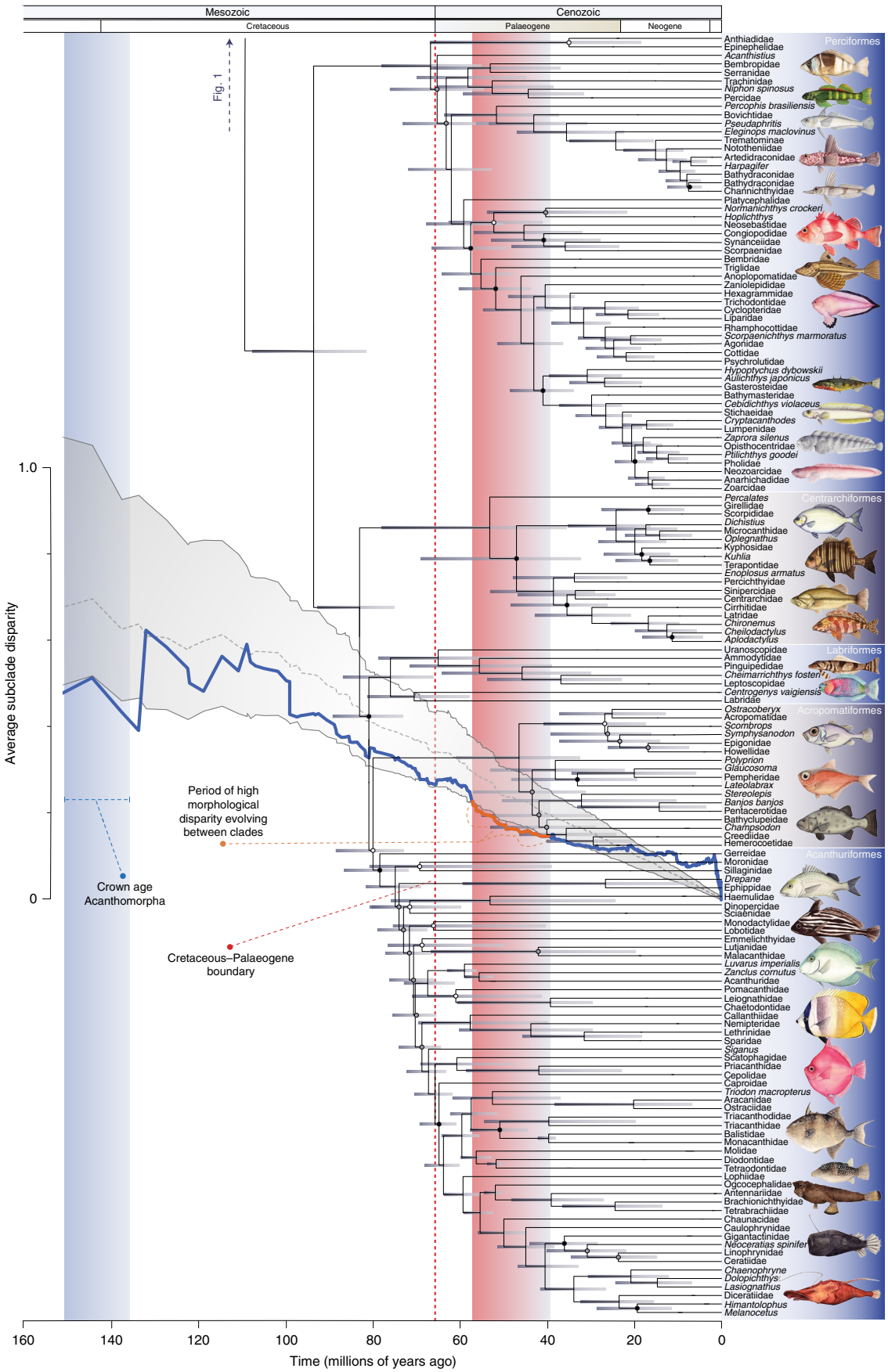
Mesozoic
Cenozoic
Cretaceous
Palaeogene
Neogene
Fig. 1
Anthiadidae
Epinephelidae
Acanthistius
Bembropidae
Serranidae
Trachinidae
Niphon spinosus
Percidae
Percophis brasiliensis
Bovichtidae
Pseudaphritis
Eleginops maclovinus
Trematominae
Nototheniidae
Artedidraconidae
Harpagifer
Bathydraconidae
Bathydraconidae
Channichthyidae
Platycephalidae
Normanichthys crockeri
Hoplichthys
Neosebastidae
Congiopodidae
Synanceiidae
Scorpaenidae
Bembridae
Triglidae
Anoplopomatidae
Zaniolepididae
Hexagrammidae
Trichodontidae
Cyclopteridae
Liparidae
Rhamphocottidae
Scorpaenichthys marmoratus
Agonidae
Cottidae
Psychrolutidae
Hypoptychus dybowskii
Aulichthys japonicus
Gasterosteidae
Bathymasteridae
Cebidichthys violaceus
Stichaeidae
Cryptacanthodes
Lumpenidae
Zaprora silenus
Opisthocentridae
Plilichthys goodei
Pholidae
Neozoarcidae
Anarhichadidae
Zoarcidae
Perciformes
Percalates
Girellidae
Scorpididae
Dichistius
Microcanthidae
Oplegnathus
Kyphosidae
Kuhlia
Terapontidae
Enoplosus armatus
Percichthyidae
Sinipercidae
Centrarchidae
Cirrhitidae
Latridae
Chironemus
Cheilodactylus
Aplodactylus
Centrarchiformes
Uranoscopidae
Ammodytidae
Pinguipedidae
Cheimarrichthys fosteri
Leptoscopidae
Centrogenys vaigiensis
Labridae
Labriformes
Ostracoberyx
Acropomatidae
Scombrops
Symphysanodon
Epigonidae
Howellidae
Polyprion
Glaucosoma
Pempheridae
Lateolabrax
Stereolepis
Banjos banjos
Pentacerotidae
Bathyclupeidae
Champsodon
Creediidae
Hemerocoetidae
Acropomatiformes
Gerreidae
Moronidae
Sillaginidae
Drepane
Ephippidae
Haemulidae
Pinguipedidae
Sciaenidae
Monodactylidae
Lobotidae
Emmelichthyidae
Lutjanidae
Malacanthidae
Luvarus imperialis
Zanclus cornutus
Acanthuridae
Pomacanthidae
Leiognathidae
Chaetodontidae
Callanthiidae
Nemipteridae
Lethrinidae
Sparidae
Siganus
Scatophagidae
Priacanthidae
Cepolidae
Caproidae
Triodon macropterus
Aracanidae
Ostraciidae
Triacanthodidae
Triacanthidae
Balistidae
Monacanthidae
Molidae
Diodontidae
Tetraodontidae
Lophiidae
Ogcocephalidae
Antennariidae
Brachionichthyidae
Tetrabrachiidae
Chaunacidae
Caulophrynidae
Gigantactinidae
Néoceratias spinifer
Linophrynidae
Ceratiidae
Chaenophryne
Dolopichthys
Lasiognathus
Diceratiidae
Himantolophus
Melanocetus
Acanthuriformes
1.0
0
Average subclade disparity
Period of high morphological disparity evolving between clades
Crown age Acanthomorpha
Cretaceous–Palaeogene boundary
160
140
120
100
80
60
40
20
0
Time (millions of years ago)

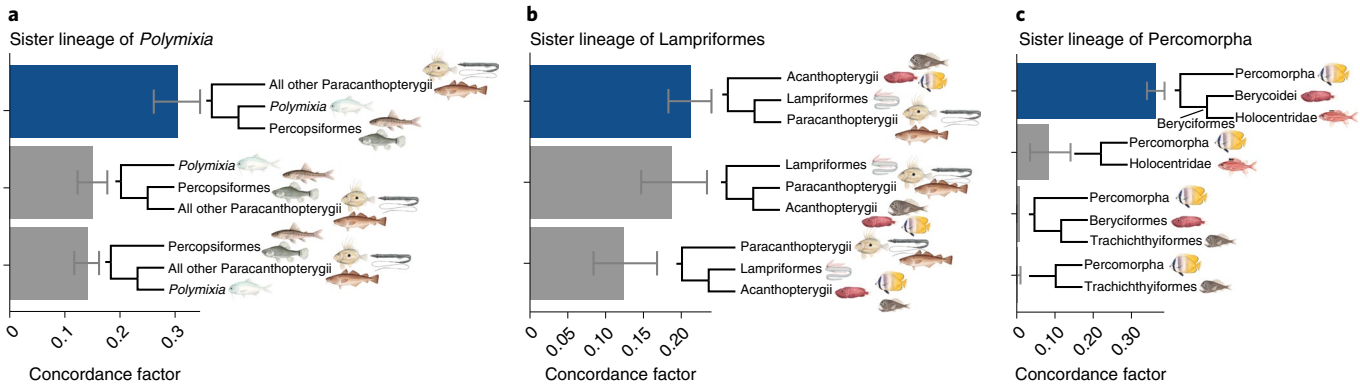

Fig. 3 | Bayesian concordance factor analyses used to compare alternative phylogenetic hypotheses concerning the sister taxa of three major acanthomorph lineages. BUCKy-inferred genome-wide posterior mean concordance factor estimates, with 95% confidence intervals, representing the proportion of $n = 250$ post-burnin gene trees exhibiting alternative topologies among major acanthomorph lineages. Lengths of blue bars reflect the posterior mean concordance factors for the topology represented in Figs. 1 and 2 and Supplementary Figs. 1–25, while lengths of grey bars represent the mean concordance factors of alternative topologies. Fish illustrations by Julie Johnson. **a**, Gene tree concordance for Percopsiformes, *Polymixia* and all other Paracanthopterygii. **b**, Lampriformes, Paracanthopterygii and Acanthopterygii. **c**, Alternative sister lineages of Percomorpha.

(sCF and gCF, respectively), or the proportion of alignment sites or gene trees in agreement with the branches in the acanthomorph phylogeny[28]. We estimate low sCF and gCF values for acanthomorph relationships that are unique to the maximum likelihood analysis of the UCE dataset, as well as for acanthomorph lineages resolved as monophyletic with strong support from other lines of evidence (Figs. 1 and 2 and Extended Data Fig. 1). However, we observe many branches with very low gCF estimates and markedly higher sCF values (Extended Data Fig. 1a), as well as a positive correlation between branch length and congruence (Extended Data Fig. 1), indicating that incomplete lineage sorting is not the sole cause of gene tree conflict[28]. Rather, the low gCF values and the observed phylogenetic incongruence are probably driven by weak phylogenetic signal in individual UCE loci, stochastic error or short subtending branches, all of which negatively impact the resolution of trees inferred from single loci[28,29]. This result is consistent with the observation that individual UCE loci contain relatively little phylogenetic information despite having higher net phylogenetic informativeness than protein-coding genes[30,31]. It also elucidates the topological differences in the phylogeny inferred using multi-species coalescent-based methods (Extended Data Fig. 2) and supports the use of concatenated alignments in our study.

As multiple processes likely drive the low gene concordance factor estimates for branches in the UCE phylogeny, low site concordance factor (sCF) values provide clearer evidence of incomplete lineage sorting. Approximately 12.8% of the UCE phylogeny's branches have higher site support for one or more alternative topologies (Figs. 1 and 2), and an additional 16.9% have sCF values similar to the site discordance factor (sDF) estimates (that is, sCF is higher than sDF by no more than 15%). The vast majority of these branches with low site support are within clades recognized as taxonomic families or represent otherwise uncontested relationships. Of note are the higher or imbalanced sDF values that highlight uncertainty in the common ancestry of Lampriformes and Paracanthopterygii (sCF 33.65%, sDF1 34.59% and sDF2 31.76%), the resolution of a clade containing Beryciformes and Percomorpha (sCF 28.63%, sDF1 46.96% and sDF2 24.41%), the identity of the earliest-diverging perciform lineages, and the resolution of Labriformes as the sister lineage of the clade comprising Acropomatiformes and Acanthuriformes (sCF 33.62%, sDF1 30.56% and sDF2 35.82%). The sDF values for several key branches within Scombriformes, Blenniiformes and Acanthuriformes are also higher than the site support for the relationships shown in Figs. 1 and 2, and there are similar sCF and sDF estimates for the branches representing the common ancestry of *Polymixia* and Percopsiformes (sCF 37.78%, sDF1 27.63% and sDF2 34.58%), as well as *Centrogenys vaigiensis* and Labridae (sCF 34.11%, sDF1 33.53% and sDF2 32.35%). Despite these uncertainties, the maximum likelihood phylogeny inferred using the concatenated dataset of the UCE loci provides an important framework for resolving the phylogenetic relationships among lineages of acanthomorph and percomorph fishes (Figs. 1 and 2).

Divergence time estimates for Acanthomorpha resulting from relaxed molecular clock analyses calibrated with 43 well-justified fossil calibrations allow for unprecedented resolution of the timing and tempo of family-level lineage diversification (Figs. 1 and 2 and Extended Data Fig. 3). The median Bayesian posterior of stem lineage age estimates demonstrates that 80% of living acanthomorph taxonomic families originated after the K–Pg, during the Palaeocene through the early Miocene (~66–15 Ma) (Extended Data Fig. 4). This pattern of an extended period of lineage origination contrasts with earlier hypotheses of a clustered origin of these percomorph lineages shortly after the K–Pg mass extinction[7]. Although most of the acanthomorph taxonomic families originated in the Palaeogene, there is an indiscernible effect of the K–Pg mass extinction on acanthomorph lineage diversification rates, as we do not detect any statistically supported mass extinctions or tree-wide rate shifts (Extended Data Fig. 5). Moreover, stepping-stone simulations, used to evaluate the relative and absolute fits of competing diversification models to the observed time-calibrated phylogeny, strongly support a constant-rate birth–death model (Extended Data Fig. 6). These analyses are not impervious to type II error, but Bayesian estimates of the evolutionary rates of individual acanthomorph lineages are similarly homogeneous across the K–Pg and through the Cenozoic (Extended Data Fig. 7). We observe increases in speciation rates in only a few percomorph clades, such as branches in the phylogeny subtending the most recent common ancestors of Apogonidae (cardinalfishes), Pseudocrenilabrinae (African cichlids), Chaetodontidae (butterflyfishes), *Sebastes* (rockfishes) and Lycodinae (a lineage of eelpouts).

Although we reconstruct a history of constant rates of lineage diversification through most of acanthomorph history, body shape began diversifying sharply at the start of the Palaeogene (Fig. 2). Our analyses of morphological disparity through time highlight a period after the K–Pg event during which mean disparity is partitioned between clades more than expected under a Brownian model of evolution (Fig. 2 and Extended Data Fig. 8), indicating a

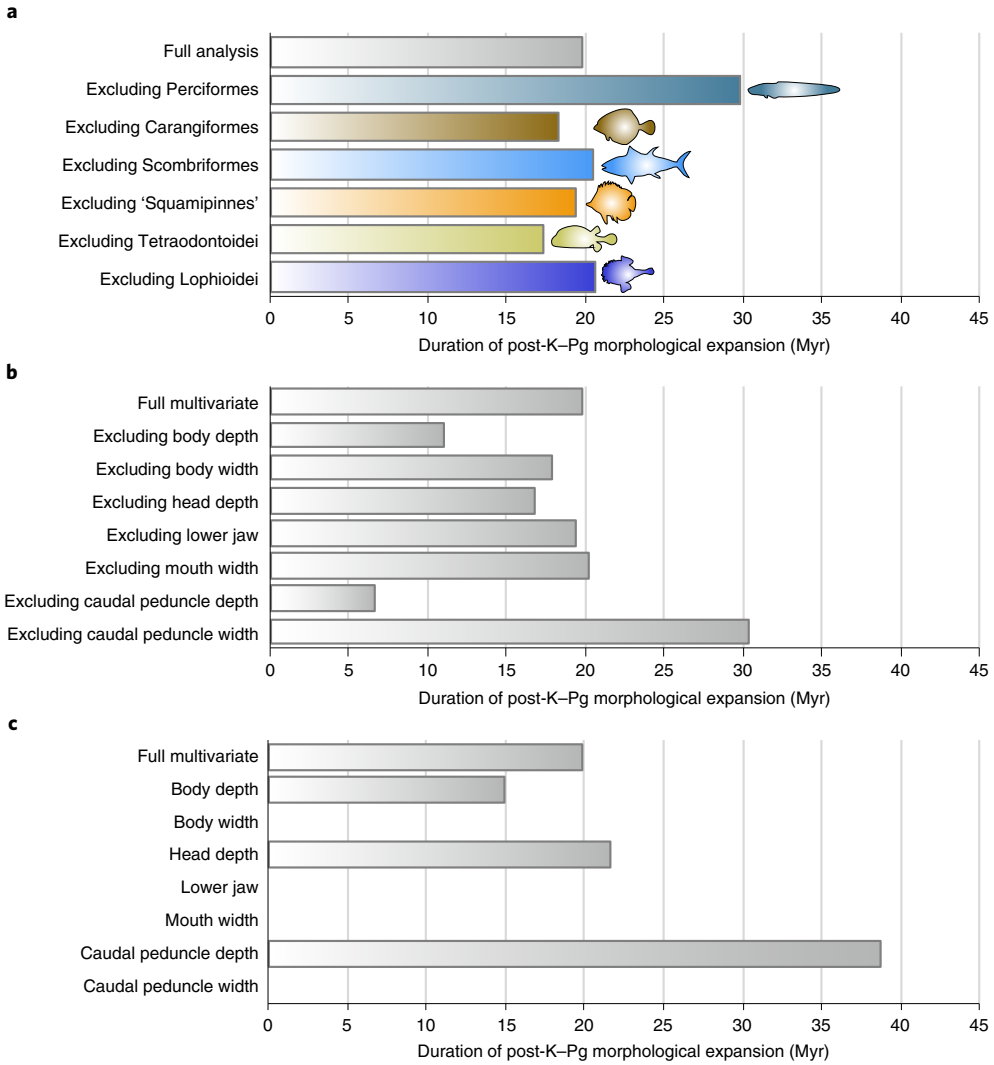

Fig. 4 | Robustness of DTT analyses. Effect of individual lineages or body shape traits on the length of the estimated period of among-clade morphological expansion after the K–Pg (that is, the period in which the observed disparity falls below that expected from a Brownian motion process). There is no single major lineage driving the duration of this period of phenotypic diversification, but the more pronounced contribution of depth measurements to this pattern indicates their importance over width measurements in the expansion of body shapes along the elongation axis. **a**, Duration of the period of morphological expansion when a single major lineage is excluded from the analysis. Note that not all major acanthomorph lineages are represented. 'Squamipinnes' refers to the acanthuriform clade in Supplementary Fig. 23 defined by *Chaetodon kleinii* and *Luvarus imperialis*, and Lophioidei and Tetraodontoidei are major subclades of Acanthuriformes. **b**, Duration of the period of morphological expansion when data for one of the seven body shape traits in the original analysis are excluded. **c**, Duration of the period of morphological expansion when the disparity through time analysis is based on a single body shape trait.

time during which subclades of Acanthomorpha evolved and maintained unique body plans[32]. This disparity through time analyses, repeated on a sample of 100 trees from the posterior distribution of BEAST time-trees, shows that the sudden diversification of acanthomorph body shapes began an average of five million years after the K–Pg and persisted until the early to mid-Eocene (~45–40 Ma) (Extended Data Fig. 8). This period of high among-clade phenotypic variation in the Palaeogene was not driven by a single clade, but occurred in several groups across Acanthomorpha (Figs. 1, 2 and 4a). The reconstructed history of phenotypic diversification is also unlikely an artefact of any topological uncertainties highlighted by the concordance factor analyses, as only 36 branches with sDF values greater than the sCF estimates bifurcate between 40 and 60 Ma. Divergences in body elongation, the lengthening of bodies relative to depth and width, contributes greatly to the pattern of the among-clade disparity detected in the disparity through time analyses (Fig. 4b,c and 5a). Elongation is one of the primary axes of body shape variation in freshwater and marine fishes[24,33], and expansion along this axis is often coupled with niche divergence and transitions between pelagic, demersal and fully benthic habitats[23,34].

During the significant expansion of acanthomorph morphological disparity in the early Palaeogene, lineages established distinct regions of morphospace that correspond to iconic present-day ecomorphological types. These forms include the bottom-dwelling, side-lying flatfishes (Pleuronectoidei) and their sister lineage of speedy, predatory, pelagic fishes (Carangoidei), both within Carangiformes (Figs. 1 and 5 and Extended Data Fig. 9). Similarly, diverse sublineages of a clade of deep-bodied fishes (Acanthuriformes) were established in the late Palaeocene and early Eocene, including globose, deep-sea anglerfishes (Lophioidei), ocean sunfishes and rotund pufferfishes (Tetraodontoidei), and laterally compressed reef fishes such as butterflyfishes (Chaetodontidae), angelfishes (Pomacanthidae) and surgeonfishes (Acanthuridae) (Fig. 2). Subsequent phenotypic evolution followed a Brownian model, as acanthomorph clades

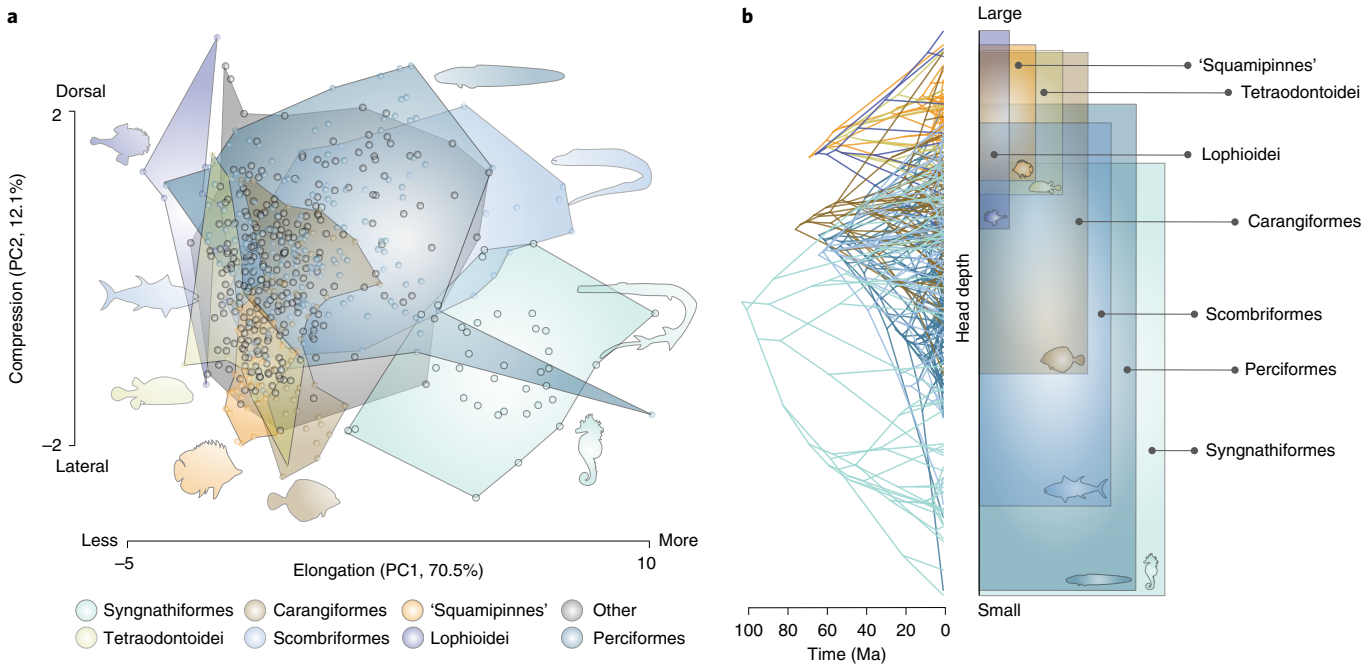

Fig. 5 | Changes in body elongation and compression. Patterns of acanthomorph morphological diversity. Note that not all major acanthomorph lineages are represented. 'Squamipinnes' refers to the acanthuriform clade in Supplementary Fig. 23 defined by *Chaetodon kleinii* and *Luvarus imperialis*, and Lophioidei and Tetraodontoidei are major subclades of Acanthuriformes. **a**, The first two principal components (PCs) of morphospace (elongation and compression), with seven major acanthomorph lineages colour-coded by taxon. The proportion of variance explained by PC1 is 70.5% and by PC2 is 12.1%. **b**, Phenogram depicting the evolutionary history of head depth (size-corrected), which is negatively correlated to standard length and can reveal patterns of elongation, across seven major acanthomorph lineages that arose around the K-Pg. Note that all major lineages except Syngnathiformes originate near the K-Pg boundary, but the three acanthuriform lineages 'Squamipinnes', Lophioidei and Tetraodontoidei have markedly different ancestral trait values from Carangiformes, Scombriformes and Perciformes.

within these well-recognized ecomorphs expanded their regions of morphospace occupation (Fig. 5b and Extended Data Fig. 9). This phenotypic diversification in some cases coincided with changes in geographic distribution and elevated rates of lineage diversification (Extended Data Fig. 7). Such a pattern is exemplified by Perciformes, which includes multiple radiations of large-mouthed predators found in habitats that range from nearshore polar habitats to tropical reefs and which repeatedly invaded both benthic and freshwater habitats. Though the evolutionary trajectories of specific spiny-rayed fish lineages are idiosyncratic (Fig. 5 and Extended Data Fig. 9), at a broader phylogenetic scale they each contribute to an overall pattern of elevated among-clade morphological disparity in Acanthomorpha during the early Cenozoic (Figs. 2 and 4 and Extended Data Fig. 8).

Our estimate of the timing of acanthomorph diversification at the onset of the Palaeogene adds an important perspective to patterns in the fossil record. Fossils suggest that acanthomorph taxonomic diversity and morphological disparity were low in the Late Cretaceous before the K–Pg event, after which both diversity and disparity increased[6,16]. The precise timing of this morphological expansion and lineage diversification remained unclear owing to a scarcity of deposits yielding abundant and well-preserved teleost skeletons between the Campanian–Maastrichtian (~72 Ma) in the Late Cretaceous and the Palaeocene–Eocene boundary (~56 Ma) (refs. [6,16]). Though isolated acanthomorph otoliths are known throughout this interval, they are not well studied relative to those from Eocene and younger deposits[35]. Our phylogenomic analyses shed light on acanthomorph diversification in the time corresponding to this gap in the fossil record, revealing that the origin of the high disparity observed among early Cenozoic fossil acanthomorphs probably began around 60 Ma and lasted for an interval of approximately 15–20 Myr. The initiation of a steady accumulation of living families and a pattern of higher among-lineage morphological disparity following the K–Pg extends through much of the gap in the acanthomorph fossil record (Fig. 2), indicating that the rise of acanthomorph diversity in the early Eocene was probably a gradual process[16].

Our results provide a new perspective to the presumed role of the K–Pg as a catalyst of vertebrate morphological and lineage diversification. We do not corroborate the observation[7] that acanthomorph lineage diversification rates increased after this global mass extinction (Extended Data Fig. 5). The approximately 15–20 Myr period following the K–Pg during which body shape trait space was highly partitioned among clades was probably coincident with the origin of much of the ecomorphological disparity that characterizes the diversity of living spiny-rayed fishes (Figs. 2 and 5b and Extended Data Figs. 8 and 9). These ecomorphological types acted as a reservoir of diversity, setting the stage for more recent, phylogenetically or geographically localized radiations, including endothermic pelagic tunas, Antarctic notothenioids, parrotfishes on coral reefs, and African Rift Lake cichlids[36–39]. Our findings indicate the remarkable diversity of spiny-rayed fishes is the product of several species-rich and morphologically disparate lineages that diversified throughout most regions of the world in nearly every available marine and freshwater habitat.

Methods

Detailed descriptions of most procedures are available in Supplementary Information.

Taxon sampling and procurement of sequence data. This study incorporates UCE sequence data from 1,109 specimens, including 9 outgroup taxa and 1,075 acanthomorph species spanning 308 recognized taxonomic families in

Acanthomorpha (Supplementary Table 1). UCE data for 360 specimens came from five previous phylogenomic studies (Supplementary Table 1), and UCE sequences for 96 species were extracted from whole genome shotgun sequence data published in the National Center for Biotechnology Information (NCBI) GenBank.

We generated new sequence data from 647 specimens representing 628 species of acanthomorphs and six outgroups, largely following the protocols for library preparation and target enrichment described by Faircloth et al.[40] and Alfaro et al.[7]. We isolated DNA from muscle or fin tissue following the standard protocol for Qiagen's DNeasy Blood and Tissue kits. After using a Qubit fluorometer (Life Technologies) to quantify 1 µl of all DNA extractions and visualizing DNA through agarose gel electrophoresis in sodium borate buffer, we sheared approximately 500 ng of genomic DNA from each sampled specimen using a QSonica Q800R3 sonicator to obtain fragment sizes between 300 and 600 nt.

We followed commercial protocols for dual indexing of genomic libraries with Kapa HyperPrep kits (Kapa Biosystems) and Illumina TruSeq iTru5 and iTru7 adapters[41]. We performed dual-step SPRI bead clean-ups with 80% EtOH washes for all purification steps, including a 0.8× clean-up after the ligation of adapters. We amplified DNA libraries using 25 µl KAPA HiFi HotStart ReadyMix (Kapa Biosystems), 5 µl of 5uM Illumina TruSeq iTru5 and iTru7 dual-indexed primers[41], and 5 µl ddH_2O using the following thermocycler settings: 98 °C for 45 s; 13 cycles of 98 °C for 15 s, 60 °C for 30 s, 72 °C for 60 s; and a final extension of 72 °C for 5 min. We purified PCR products using 1.0× SPRI beads and rehydrated libraries in 25 µl of 10 mM Tris–HCl. After library quantification with a Qubit flourometer, we pooled 80 ng of each sample into groups of nine, dried the pools in a vacuufuge and rehydrated with 4.9 µl of 10 mM Tris–HCl.

We used a bait set from Arbor Biosciences designed to target 1,314 UCE loci in acanthomorph fishes for target enrichment of UCE loci[7]. For 24 h at 65 °C, we allowed pooled libraries to hybridize with 100 ng Arbor Biosciences myBaits, 500 ng custom blocking oligos, 500 ng commercially available human Cot-1 DNA (Arbor Biosciences) and 1% sodium dodecyl sulfate. After hybrid enrichment, we performed 2.0× bead clean-ups on all pools, during which we removed all residue of the final wash buffer, allowed samples to dry on the magnetic rack and rehydrated samples with 30 µl of ddH_2O. We combined these bead-bound enriched libraries with 25 µl HiFi HotStart ReadyMix polymerase (Kapa Biosystems), 5 µl of each Illumina TruSeq primer mix and 5 µl ddH_2O. Samples then underwent a PCR with 16 amplification cycles using the same temperature and time settings that were used earlier for library amplification. We performed 1.0× bead clean-ups to purify the reaction products, and rehydrated pools in 33 µl ddH_2O. We quantified the enriched pools, diluted them to 2.5 ng µl^{-1}, affirmed their size distribution using a Bioanalyzer (Agilent Technologies) and quantified each pool via qPCR using a commercial kit (Kapa Biosystems). Using the Bioanalyzer's estimates of mean fragment sizes and the qPCR results, we adjusted sample concentrations to 10 nM and created an equimolar pool of all enriched libraries. Libraries were sequenced using 150 bp paired-end sequencing on Illumina HiSeq platforms.

Data processing and phylogenetic analyses. We used the PHYLUCE v.1.7.1 (refs. [40,42]) computer package to process raw read data, remove potential paralogues, conduct de novo assembly and construct alignments of UCE loci. We generated two separate alignments of UCE loci present in at least 75% of the samples: one consisting of all 1,109 specimens (1,084 species) and another including only a subset of the 702 species that overlapped with the taxon sampling of a previously published morphological dataset. The 1,084- and 702-taxon alignments consisted of 987 loci (383,250 bp) and 989 loci (499,957 bp), respectively.

Using these two 75% complete data matrices, we conducted multiple phylogenetic analyses using maximum likelihood methods in IQ-TREE v.1.7 (ref. [43]) and RAxML-ng v.0.9.0 (ref. [44]). We topologically constrained the divergence time analyses represented in Figs. 1 and 2 with phylogenies inferred in IQ-TREE using single-partition alignments of the 702-taxon and 1,084-taxon datasets. Both of these tree searches assumed the GTR + Gamma model of molecular evolution and used ultrafast bootstrap approximation to generate 1,000 bootstrap replicates and 1,000 replicates of the Shimodaira–Hasegawa approximate likelihood ratio test (SH-aLRT). We used the program TOPD v.4.6 (ref. [45]) to ensure the phylogenies inferred using different partitioning schemes and maximum likelihood programs presented similar tree topologies.

We also used IQ-TREE's ModelFinder Plus and ultrafast bootstrap approximation options to infer maximum likelihood gene trees for each UCE locus. In TreeShrink[46], we used a false-positive tolerance rate parameter (α) of 0.05 to identify and remove potentially aberrant sequences from the single-gene alignments. We re-aligned filtered alignments using MAFFT v.7.130b (ref. [47]) and used them to repeat inference of gene trees in IQ-TREE. We employed the resulting gene trees to generate a summary species tree in ASTRAL-III v.5.6.3 (ref. [48]). Additionally, we applied these gene trees in IQ-TREE 2 (ref. [49]) to calculate the percentage of decisive gene trees (gCF) that are consistent with each branch in the single-partition IQ-TREE phylogeny[28]. To calculate stable sCF values for every internal branch, we randomly subsampled 100 quartets from our concatenated alignment. We performed correlation analyses between branch lengths and maximum likelihood concordance factor values using base R functions after log-transforming branch lengths (results in the legend of Extended Data Fig. 1).

We also applied Bayesian methods to understand the degree of topological discordance along the backbone of the acanthomorph tree. For an 82-taxon sample that represented the major acanthomorph subclades, we generated alignments using MAFFT and inferred gene tree distributions for each locus. We ran these tree searches in MrBayes v.3.2.7 (ref. [50]) for 2 million generations, assuming a GTR + Gamma model of molecular evolution. We measured topological discordance between these Bayesian gene trees by estimating genome-wide concordance factors in BUCKy[51] using an α value of 1.0.

Divergence time estimation. We estimated divergence times for the 702- and 1,084-taxon phylogenies in BEAST v.2.5 (refs. [52–54]) using reduced datasets of randomly subsampled UCE loci[36,55]. For both phylogenies, we repeated dating analyses on three different alignments of 30 loci. For each of these alignments, we accounted for site-specific variation in evolutionary patterns by selecting the best-fit partitioning schemes using PartitionFinder2 v.2.1.1 (ref. [56]). We performed at least three replicate analyses for each 30-locus dataset. We ran all BEAST analyses under a relaxed log-normal clock model and a birth–death tree model, using the IQ-TREE phylogenies inferred from the single-partition, 702- and 1,084-taxon alignments as topological constraints. We used 43 fossil constraints (detailed in Supplementary Information) to assign minimum age priors and ran BEAST analyses for a minimum of 200 million generations after discarding a burnin of 200 million iterations. We used Tracer v.1.7.1 (ref. [57]) to assess convergence of parameters across replicate MCMC chains and ensure there were no directional trends in parameter estimates. For each set of random loci, we combined replicate analyses in LogCombiner and constructed maximum clade credibility (MCC) trees using TreeAnnotator in BEAST v.1.8.4 (ref. [58]), with summarized node heights rescaled to reflect the posterior median heights. MCC trees for the 702-taxon datasets were summarized from 10,000 post-burnin, randomly sampled trees, while MCC trees for the 1,084-taxon datasets were summarized from 1,200 such trees.

Diversification rate analyses. We removed all outgroup and duplicate taxa from the 1,084-taxon MCC tree displaying the highest effective sample size and used this pruned tree for all diversification rate analyses. We used TESS[59] to conduct stepping-stone simulations that estimated the marginal likelihoods of eight birth–death models, allowing us to calculate Bayes factors and assess the competing models' relative and absolute fits to the time-calibrated phylogeny of Acanthomorpha. We examined tree-wide speciation, extinction and net-diversification rates using TESS's CoMET model. For this analysis, we accounted for our incomplete sampling, specified a uniform sampling strategy and ran three replicate reversible-jump MCMC chains until effective sample size values were ≥200. CoMET runs were checked for within- and between-analysis convergence of the diversification rate parameters as described in Supplementary Information. Using the same time-calibrated phylogeny, we also inferred rate heterogeneity across lineages using BAMM v.2.5.0 (ref. [60]). BAMM analyses accounted for the incomplete sampling of taxonomic families and other major representative clades and used empirically determined rate priors identified by the R package BAMMtools v.2.1.6 (ref. [61]). We ran 23 MCMC chains with different combinations of parameters in BAMM, each for 100 million generations, and we identified the rate shifts along specific branches that were predicted by at least 16 of these analyses.

Phylogenetic comparative methods. We pruned a body trait dataset of teleost fishes[24] to include maximum body depth, maximum fish width, head depth, lower jaw length, mouth width, minimum caudal peduncle depth and minimum caudal peduncle width for the 680 species that matched the species represented in the 702-taxon UCE phylogeny. To correct for body size, we regressed log-transformed trait values against log-transformed standard fish lengths and calculated phylogenetic residuals in PHYTOOLS[62]. We assessed disparity through time using GEIGER[63] and the time-calibrated IQ-TREE phylogeny. We repeated disparity through time analyses on 100 randomly sampled time trees from the posterior distribution generated in BEAST, and we summarized the mean and 95% confidence interval for the 1.0 My time interval after the K–Pg during which average subclade disparity first dropped below the value simulated under Brownian evolution, as well as the proportion of trees through time that strayed from the Brownian prediction. We tested the sensitivity of disparity through time analyses to the exclusion of body shape traits and of major clades that arose immediately around the K–Pg boundary. Finally, we used PHYTOOLS to visualize body shape morphospace using principal component analysis and to generate phenograms that visualize the evolutionary histories of the following seven major lineages: Scombriformes, Syngnathiformes, Carangiformes, Perciformes, Lophioidei (in Acanthuriformes), Tetraodontoidei (in Acanthuriformes) and 'Squamipinnes' (referring to the acanthuriform clade in Supplementary Fig. 23 defined by *Chaetodon kleinii* and *Luvarus imperialis*).

Reporting summary. Further information on research design is available in the Nature Research Reporting Summary linked to this article.

Data availability

NCBI BioSample Accession numbers corresponding to sequence data are listed in Supplementary Table 1. New raw sequence data are available for download from the NCBI Sequence Read Archive (SRA), under BioProject ID PRJNA758064.

Sequence alignments, partitioning schemes, phylogenetic trees, phenotypic trait data and other related data files are available on the corresponding Dryad Digital Repository: https://datadryad.org/stash/share/-vfd5XqnNuJ1BHG7s2nBDw2nRRyK80Rc4BAtkrAkkoU.

Code availability

Analyses relied on open-source programs, and scripts used for data analysis are available on the Dryad Digital Repository: https://datadryad.org/stash/share/-vfd5XqnNuJ1BHG7s2nBDw2nRRyK80Rc4BAtkrAkkoU.

Received: 6 May 2021; Accepted: 19 May 2022;
Published online: 14 July 2022

References

1. Fricke, R., Eschmeyer, W. N. & Fong, J. D. *Eschmeyer's Catalog of Fishes: species by family/subfamily (1 September 2021)* https://researcharchive.calacademy.org/research/ichthyology/catalog/SpeciesByFamily.asp (2021).
2. Wainwright, P. C. & Longo, S. J. Functional innovations and the conquest of the oceans by acanthomorph fishes. *Curr. Biol.* **27**, R550–R557 (2017).
3. Near, T. J. et al. Phylogeny and tempo of diversification in the superradiation of spiny-rayed fishes. *Proc. Natl Acad. Sci. USA* **110**, 12738–12743 (2013).
4. Dornburg, A. & Near, T. J. The emerging phylogenetic perspective on the evolution of actinopterygian fishes. *Annu. Rev. Ecol., Evolution, Syst.* **52**, 427–452 (2021).
5. Chen, W.-J. et al. New insights on early evolution of spiny-rayed fishes (Teleostei: Acanthomorpha). *Front. Mar. Sci.* **1**, 53 (2014).
6. Friedman, M. Explosive morphological diversification of spiny-finned teleost fishes in the aftermath of the end-Cretaceous extinction. *Proc. R. Soc. B* **277**, 1675–1683 (2010).
7. Alfaro, M. E. et al. Explosive diversification of marine fishes at the Cretaceous–Palaeogene boundary. *Nat. Ecol. Evolution* **2**, 688–696 (2018).
8. Meredith, R. W. et al. Impacts of the Cretaceous terrestrial revolution and KPg extinction on mammal diversification. *Science* **334**, 521–524 (2011).
9. Stadler, T. Mammalian phylogeny reveals recent diversification rate shifts. *Proc. Natl Acad. Sci. USA* **108**, 6187–6192 (2011).
10. Venditti, C., Meade, A. & Pagel, M. Multiple routes to mammalian diversity. *Nature* **479**, 393–396 (2011).
11. Liu, L. et al. Genomic evidence reveals a radiation of placental mammals uninterrupted by the KPg boundary. *Proc. Natl Acad. Sci. USA* **114**, E7282–E7290 (2017).
12. Slater, G. J. Phylogenetic evidence for a shift in the mode of mammalian body size evolution at the Cretaceous–Palaeogene boundary. *Methods Ecol. Evol.* **4**, 734–744 (2013).
13. Jetz, W. & Pyron, R. A. The interplay of past diversification and evolutionary isolation with present imperilment across the amphibian tree of life. *Nat. Ecol. Evolution* **2**, 850–858 (2018).
14. Longrich, N. R., Bhullar, B.-A. S. & Gauthier, J. Mass extinction of lizards and snakes at the Cretaceous–Paleogene boundary. *Proc. Natl Acad. Sci. USA* **109**, 21396–21401 (2012).
15. Jarvis, E. D. et al. Whole-genome analyses resolve early branches in the tree of life of modern birds. *Science* **346**, 1320 (2014).
16. Patterson, C. An overview of the early fossil record of acanthomorphs. *Bull. Mar. Sci.* **52**, 29–59 (1993).
17. Betancur-R, R. et al. The tree of life and a new classification of bony fishes. *PLOS Curr.* https://doi.org/10.1371/currents.tol.53ba26640df0ccaee75bb165c8c26288 (2013).
18. Hughes, L. C. et al. Comprehensive phylogeny of ray-finned fishes (Actinopterygii) based on transcriptomic and genomic data. *Proc. Natl Acad. Sci. USA* **115**, 6249–6254 (2018).
19. Johnson, G. D. & Patterson, C. Percomorph phylogeny: a survey of acanthomorphs and a new proposal. *Bull. Mar. Sci.* **52**, 554–626 (1993).
20. Near, T. J. et al. Resolution of ray-finned fish phylogeny and timing of diversification. *Proc. Natl Acad. Sci. USA* **109**, 13698–13703 (2012).
21. Miya, M. et al. Major patterns of higher teleostean phylogenies: a new perspective based on 100 complete mitochondrial DNA sequences. *Mol. Phylogenet. Evol.* **26**, 121–138 (2003).
22. Wainwright, P. C. et al. The evolution of pharyngognathy: a phylogenetic and functional appraisal of the pharyngeal jaw key innovation in labroid fishes and beyond. *Syst. Biol.* **61**, 1001–1027 (2012).
23. Ribeiro, E., Davis, A. M., Rivero-Vega, R. A., Ortí, G. & Betancur-R, R. Post-Cretaceous bursts of evolution along the benthic-pelagic axis in marine fishes. *Proc. R. Soc. B* **285**, 20182010 (2018).
24. Price, S. A. et al. Building a body shape morphospace of teleostean fishes. *Integ. Comp. Biol.* **59**, 716–730 (2019).
25. Smith, W. L., Stern, J. H., Girard, M. G. & Davis, M. P. Evolution of venomous cartilaginous and ray-finned fishes. *Integ. Comp. Biol.* **56**, 950–961 (2016).
26. Liem, K. Evolutionary strategies and morphological innovations: cichlid pharyngeal jaws. *Syst. Zool.* **22**, 425–441 (1973).
27. Chan, K. O., Hutter, C. R., Wood, P. L., Grismer, L. L. & Brown, R. M. Larger, unfiltered datasets are more effective at resolving phylogenetic conflict: Introns, exons, and UCEs resolve ambiguities in Golden-backed frogs (Anura: Ranidae; genus *Hylarana*). *Mol. Phylogenet. Evol.* **151**, 106899 (2020).
28. Minh, B. Q., Hahn, M. W. & Lanfear, R. New methods to calculate concordance factors for phylogenomic datasets. *Mol. Biol. Evol.* **37**, 2727–2733 (2020).
29. Simion, P., Delsuc, F. & Philippe, H. in *Phylogenetics in the genomic era* (eds C. Scornavacca, F. Delsuc & N. Galtier) 2.1:1–2.1:34 (no commercial publisher, authors open access book, 2020).
30. Gilbert, P. S. et al. Genome-wide ultraconserved elements exhibit higher phylogenetic informativeness than traditional gene markers in percomorph fishes. *Mol. Phylogenet. Evol.* **92**, 140–146 (2015).
31. Alda, F., Ludt, W. B., Elías, D. J., McMahan, C. D. & Chakrabarty, P. Comparing ultraconserved elements and exons for phylogenomic analyses of Middle American cichlids: when data agree to disagree. *Genome Biol. Evol.* https://doi.org/10.1093/gbe/evab161 (2021).
32. Harmon, L. J., Schulte, J. A., Larson, A. II & Losos, J. B. Tempo and mode of evolutionary radiation in iguanian lizards. *Science* **301**, 961–964 (2003).
33. Claverie, T. & Wainwright, P. C. A morphospace for reef fishes: elongation Is the dominant axis of body shape evolution. *PLoS ONE* **9**, e112732 (2014).
34. Friedman, S. T. et al. Body shape diversification along the benthic–pelagic axis in marine fishes. *Proc. R. Soc. B* **287**, 20201053 (2020).
35. Schwarzhans, W. & Stringer, G. Fish otoliths from the Late Maastrichtian Kemp Clay (Texas, USA) and the Early Dannian Clayton Formation (Arkansas, USA) and an assessment of extinction and survival of teleost lineages across the K–Pg boundary based on otoliths. *Riv. Ital. Paleontol. Strat.* **126**, 395–446 (2020).
36. Friedman, M. et al. A phylogenomic framework for pelagiarian fishes (Acanthomorpha: Percomorpha) highlights mosaic radiation in the open ocean. *Proc. R. Soc. B* **286**, 20191502 (2019).
37. Price, S. A., Holzman, R., Near, T. J. & Wainwright, P. C. Coral reefs promote the evolution of morphological diversity and ecological novelty in labrid fishes. *Ecol. Lett.* **14**, 462–469 (2011).
38. McGee, M. D. et al. The ecological and genomic basis of explosive adaptive radiation. *Nature* **586**, 75–79 (2020).
39. Daane, J. M. et al. Historical contingency shapes adaptive radiation in Antarctic fishes. *Nat. Ecol. Evolution* https://doi.org/10.1038/s41559-019-0914-2 (2019).
40. Faircloth, B. C. et al. Ultraconserved elements anchor thousands of genetic markers spanning multiple evolutionary timescales. *Syst. Biol.* **61**, 717–726 (2012).
41. Glenn, T. C. et al. Adapterama I: universal stubs and primers for 384 unique dual-indexed of 147,456 combinatorially-indexed Illumina libraries (iTru & iNext). *PeerJ* **7**, e7755 (2019).
42. Faircloth, B. C. PHYLUCE is a software package for the analysis of conserved genomic loci. *Bioinformatics* **32**, 786–788 (2016).
43. Nguyen, L. T., Schmidt, H. A., von Haeseler, A. & Minh, B. Q. IQ-TREE: a fast and effective stochastic algorithm for estimating maximum likelihood phylogenies. *Mol. Biol. Evol.* **32**, 268–274 (2015).
44. Kozlov, A. M., Darriba, D., Flouri, T., Morel, B. & Stamatakis, A. RAxML-NG: a fast, scalable and user-friendly tool for maximum likelihood phylogenetic inference. *Bioinformatics* **35**, 4453–4455 (2019).
45. Puigbò, P., Garcia-Vallvé, S. & McInerney, J. O. TOPD/FMTS: a new software to compare phylogenetic trees. *Bioinformatics* **23**, 1556–1558 (2007).
46. Mai, U. & Mirarab, S. TreeShrink: fast and accurate detection of outlier long branches in collections of phylogenetic trees. *BMC Genomics* **19**, 23–40 (2018).
47. Katoh, K. & Standley, D. M. MAFFT multiple sequence alignment software Version 7: improvements in performance and usability. *Mol. Biol. Evol.* **30**, 772–780 (2013).
48. Zhang, C., Rabiee, M., Sayyari, E. & Mirarab, S. ASTRAL-III: polynomial time species tree reconstruction from partially resolved gene trees. *BMC Bioinformatics* **19**, 15–30 (2018).
49. Minh, B. Q. et al. IQ-TREE 2: new models and efficient methods for phylogenetic inference in the genomic era. *Mol. Biol. Evol.* **37**, 1530–1534 (2020).
50. Ronquist, F. et al. MrBayes 3.2: efficient Bayesian phylogenetic inference and model choice across a large model space. *Syst. Biol.* **61**, 539–542 (2012).
51. Ane, C., Larget, B., Baum, D. A., Smith, S. D. & Rokas, A. Bayesian estimation of concordance among gene trees. *Mol. Biol. Evol.* **24**, 412–426 (2007).
52. Bouckaert, R. et al. BEAST 2.5: an advanced software platform for Bayesian evolutionary analysis. *PLoS Comput. Biol.* **15**, e1006650 (2019).
53. Gernhard, T. The conditioned reconstructed process. *J. Theor. Biol.* **253**, 769–778 (2008).
54. Drummond, A. J., Ho, S. Y. W., Phillips, M. J. & Rambaut, A. Relaxed phylogenetics and dating with confidence. *PLoS Biol.* **4**, 699–710 (2006).

55. Harrington, R. C. et al. Phylogenomic analysis of carangimorph fishes reveals flatfish asymmetry arose in a blink of the evolutionary eye. *BMC Evol. Biol.* **16**, 224 (2016).
56. Lanfear, R., Frandsen, P. B., Wright, A. M., Senfeld, T. & Calcott, B. PartitionFinder 2: new methods for selecting partitioned models of evolution for molecular and morphological phylogenetic analyses. *Mol. Biol. Evol.* **34**, 772–773 (2017).
57. Rambaut, A., Drummond, A. J., Xie, D., Baele, G. & Suchard, M. A. Posterior summarization in Bayesian phylogenetics using Tracer 1.7. *Syst. Biol.* **67**, 901–904 (2018).
58. Drummond, A. J., Suchard, M. A., Xie, D. & Rambaut, A. Bayesian phylogenetics with BEAUti and the BEAST 1.7. *Mol. Biol. Evol.* **29**, 1969–1973 (2012).
59. Höhna, S., May, M. R. & Moore, B. R. TESS: an R package for efficiently simulating phylogenetic trees and performing Bayesian inference of lineage diversification rates. *Bioinformatics* **32**, 789–791 (2016).
60. Rabosky, D. L. Automatic detection of key innovations, rate shifts, and diversity-dependence on phylogenetic trees. *PLoS ONE* **9**, e89543 (2014).
61. Rabosky, D. L. et al. BAMMtools: an R package for the analysis of evolutionary dynamics on phylogenetic trees. *Methods Ecol. Evol.* **5**, 701–707 (2014).
62. Revell, L. J. phytools: an R package for phylogenetic comparative biology (and other things). *Methods Ecol. Evol.* **3**, 217–223 (2012).
63. Harmon, L. J., Weir, J. T., Brock, C. D., Glor, R. E. & Challenger, W. GEIGER: investigating evolutionary radiations. *Bioinformatics* **24**, 129–131 (2008).

Acknowledgements

We thank J. Johnson for the fish illustrations in Figs. 1–3 and Extended Data Fig. 3, and the numerous undergraduate and graduate researchers from the University of California, Davis and Clemson University who helped collect morphological data. Portions of this research were conducted with high-performance computational resources provided by Louisiana State University (http://www.hpc.lsu.edu). We are grateful to the ichthyology curators and staff of the following collections for granting access to the tissues and specimens that made this study possible: Smithsonian National Museum of Natural History (Washington, DC), University of Florida Museum of Natural History (Gainesville), Scripps Institution of Oceanography (La Jolla), South African Institute for Aquatic Biodiversity (Grahamstown), Southeastern Louisiana University Museum of Biology (Hammond), American Museum of Natural History (New York), Australian Museum (Sydney), Academy of Natural Sciences (Philadelphia), Field Museum of Natural History (Chicago), California Academy of Sciences (San Francisco), Cornell University Museum of Vertebrates (Ithaca), University of Tennessee David A. Etnier Ichthyological Collection (Knoxville), Burke Museum of Natural History and Culture (Seattle), Academia Sinica (Taipei), Biodiversity Research Museum (Taipei), Natural History Museum and Institute (Chiba), Australian National Fish Collection (Hobart), Kyoto University Museum, Mie University Fish Collection of the Fisheries Research Laboratory (Shima), Hokkaido University Museum (Sapporo), Illinois Natural History Survey (Champaign), Kagoshima University Museum (Korimoto), University of Kansas Biodiversity Institute (Lawrence), Natural History Museum of Los Angeles County, Universidade Estadual Paulista (São Paulo), Louisiana Museum of Natural History (Baton Rouge), Harvard Museum of Comparative Zoology (Cambridge), Museo Nacional de Ciencias Naturales (Madrid), Museo Nacional de Historia Natural (Santiago), North Carolina Museum of Natural Sciences (Raleigh), National Museum of Natural History (New Delhi), Museum of New Zealand Te Papa Tongarewa (Wellington), Museum Victoria (Melbourne), National Museum of Nature and Science (Tokyo), Museums and Art Galleries of the Northern Territory (Darwin), University of Tokyo Ocean Research Institute, Queensland Museum (Brisbane), Royal Ontario Museum (Toronto), Seikai National Fisheries Research Institute (Nagasaki), Universitetsmuseet i Bergen (Hordaland), University of Copenhagen Zoological Museum, and Peabody Museum of Natural History (New Haven). Funding: Authors were independently funded by the National Institute of Health Predoctoral Training Program in Genetics T32 GM 007499 (to A.G.), the Bingham Oceanographic Fund maintained by the Peabody Museum of Natural History, Yale University (to T.J.N.), the Australian Research Council DECRA Fellowship DE170100516 (to P.F.C.), start-up funds from Louisiana State University (to B.C.F.) and the following National Science Foundation grants: NSF DEB-1556953 (to S.A.P. and P.C.W.), NSF DEB-1655624 (to B.C.F.), NSF DEB-1701323 (to P.C. and W.B.L.), NSF DEB-1830127 (to S.A.P.), NSF DEB-1839915 (to P.C.), NSF DEB-2017822 (to M.F.) and NSF IOS-1755242 (to A.D.).

Author contributions

The project was conceived and designed by T.J.N., A.G., R.C.H., J.R.G., B.C.F. and P.C.W. A.G., R.C.H., J.R.G., M.A.C., J.C.B., W.T.M., M.E.A., W.B.L., B.C.F., P.F.C. and T.J.N. organized and executed the collection of UCE sequence data. S.A.P., S.T.F. and P.C.W. coordinated and collected morphological data. A.G., R.C.H., B.C.F. and A.D. carried out phylogenetic analyses. A.G. and R.C.H. performed phylogenetic divergence dating analyses, and A.G. performed analyses of lineage diversification rates. E.D.B. and P.C.W. performed morphological comparative analyses. C.E.T., P.C., W.B.L., P.F.C., P.J.U., A.D. and B.C.F. aided in the interpretation of certain phylogenetic or taxonomic results, and M.F. contributed palaeontological insights into some results. A.G., R.C.H., A.D. and T.J.N. wrote the first draft of the manuscript. All authors contributed to the writing and editing of the final draft of the manuscript.

Competing interests

The authors declare no competing interests.

Additional information

Extended data is available for this paper at https://doi.org/10.1038/s41559-022-01801-3.

Supplementary information The online version contains supplementary material available at https://doi.org/10.1038/s41559-022-01801-3.

Correspondence and requests for materials should be addressed to Ava Ghezelayagh or Richard C. Harrington.

Peer review information *Nature Ecology & Evolution* thanks Ole Seehausen and the other, anonymous, reviewer(s) for their contribution to the peer review of this work.

Reprints and permissions information is available at www.nature.com/reprints.

Publisher's note Springer Nature remains neutral with regard to jurisdictional claims in published maps and institutional affiliations.

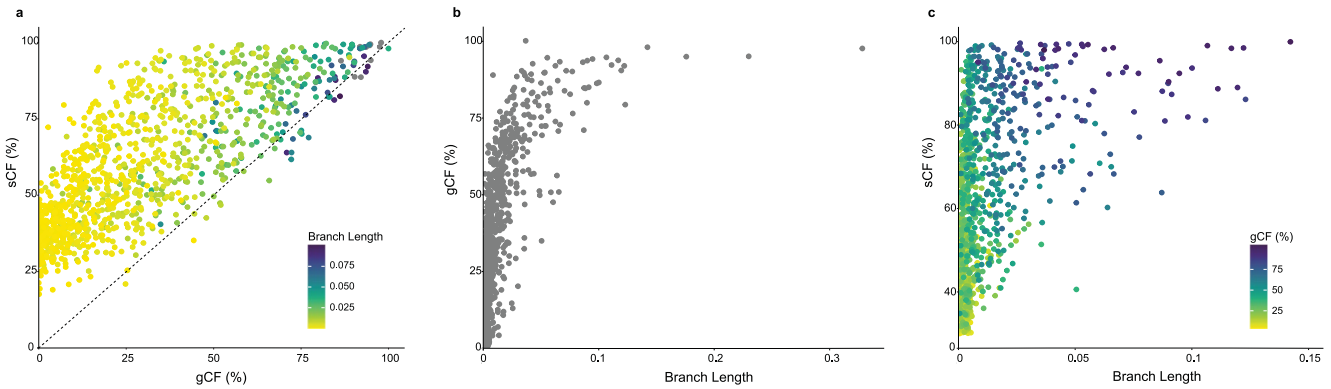

Extended Data Fig. 1 | Relationships among gene concordance factor (gCF) values, site concordance factor values (sCF) and branch lengths (substitutions per sequence site) along all branches of the acanthomorph phylogeny represented in Supplementary Figs. 1–25. Note that unlike gCF values, site concordance and discordance values sum to 100% because their calculations allow for only three possible resolutions of a branch. Branch lengths have a positive, logarithmic correlation with gCF and sCF. A one percent increase in branch lengths leads to a 0.1413 increase in the natural log of gCF (Standard Error = 0.2925, y-intercept = 108.3323, R-squared = 0.6791) and a 0.0905 change in the natural log of sCF (Standard Error = 0.3416, y-intercept = 109.851, R-squared = 0.3889). These correlation analyses were performed using base R functions after log-transforming branch lengths; all branches were included in these calculations. **a**, Relationship between gCF and sCF, with points colored by branch lengths. The dashed black line with a slope of 1 demonstrates dissimilar levels of conflict among loci and sites, suggesting that the low gCF values are not just caused by genuine discordance in the gene trees. Eleven gray points reflect extremely long branches with lengths greater than 0.1 nucleotide substitutions per site (greater than the upper 99th percentile). **b**, Logarithmic relationship between branch lengths and gCF. **c**, Relationship between branch lengths and sCF values, with points colored by gCF values. Not shown are three points with very long branches (0.176-0.328 substitutions per sequence sites), all of which have sCF and gCF values >94%.

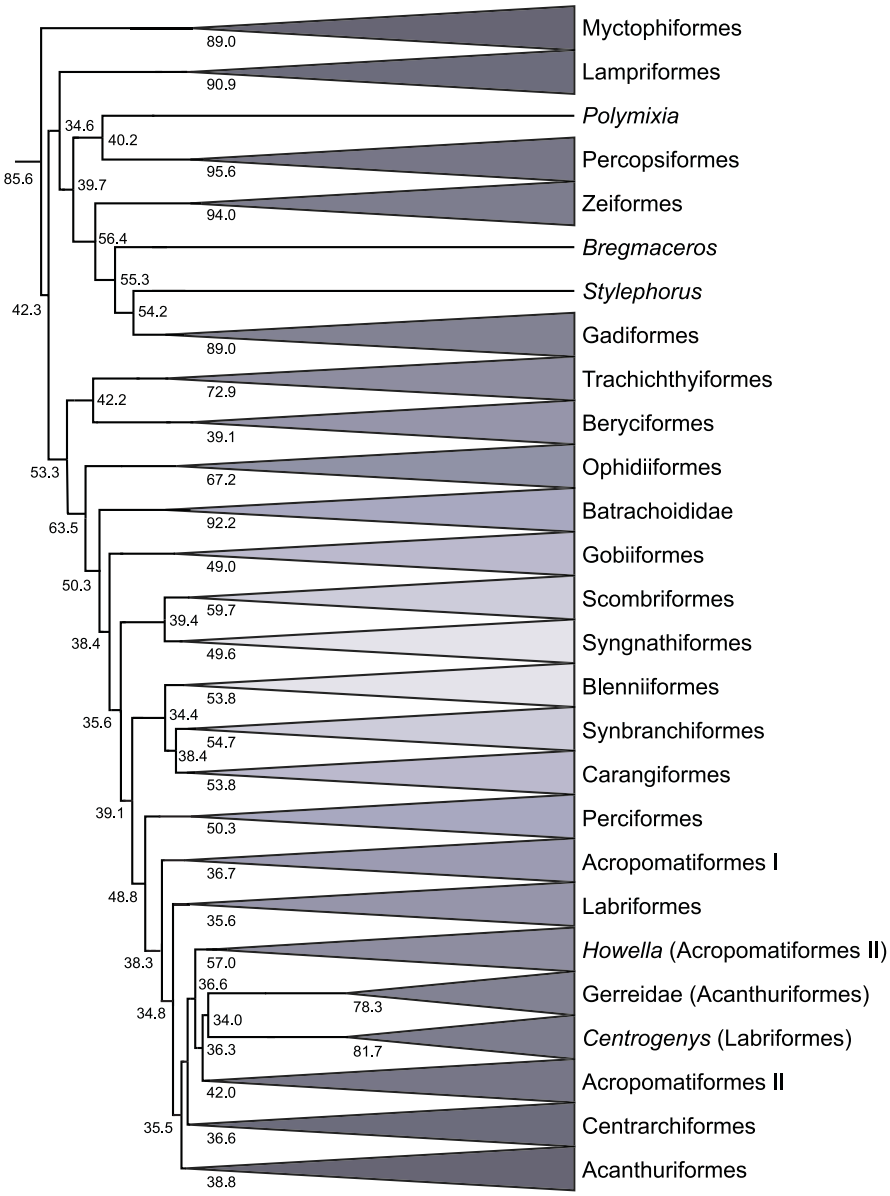

Extended Data Fig. 2 | ASTRAL-III summary species tree inferred using individual gene trees. Collapsed species tree inferred under the multi-species coalescent model (the uncollapsed tree can be found in the study's Dryad repository). Local posterior probability values at nodes do not measure support for bipartitions, but rather are a function of the frequencies of the represented quartet topologies among all gene trees. 'Acropomatiformes I' refers to the clade containing *Champsodon*, Creediidae, and Hemerocoetidae while 'Acropomatiformes II' includes all other acropomatiform taxa according to Supplementary Table 3.

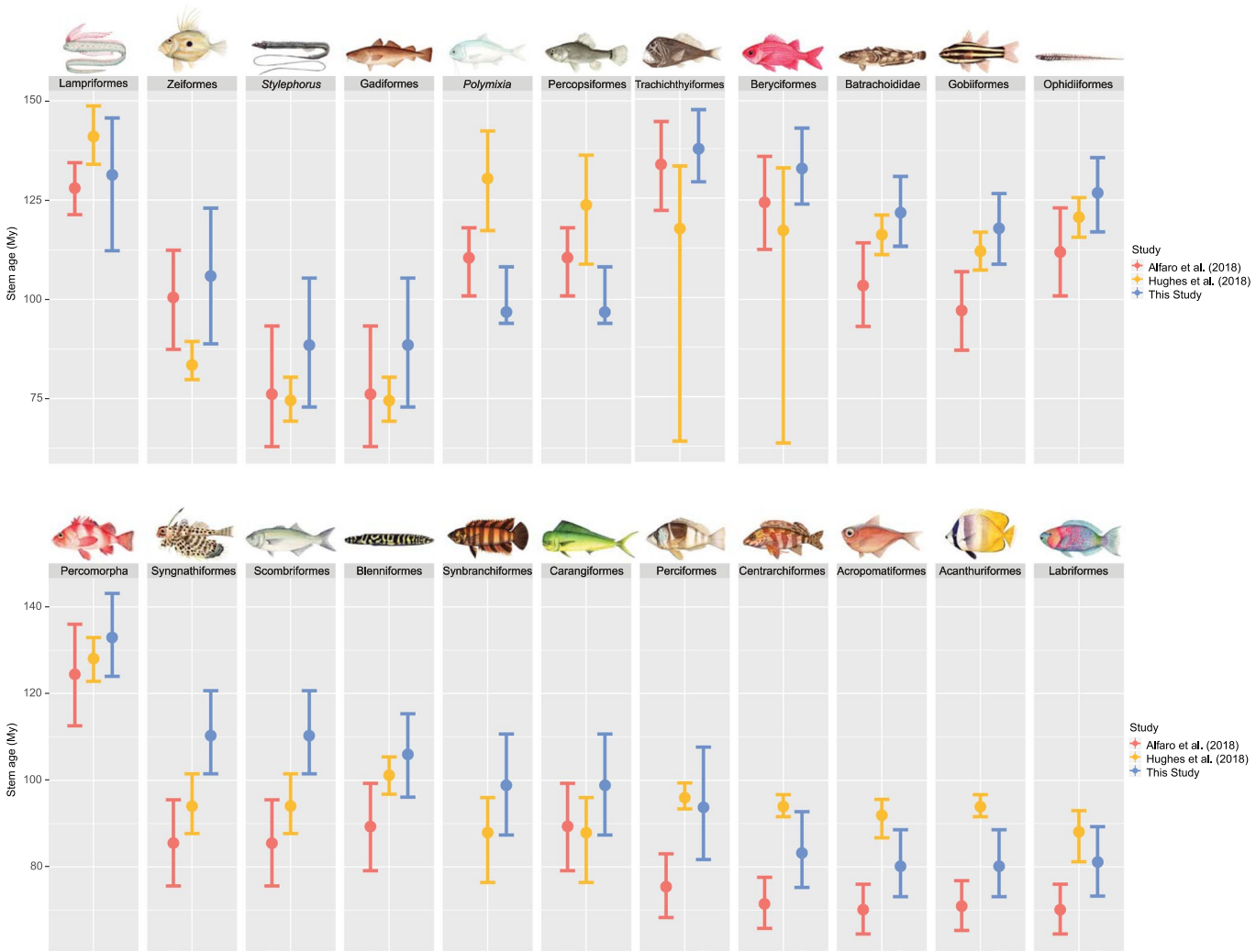

Extended Data Fig. 3 | Median stem age estimates and 95% Highest Posterior Density (HPD) credible intervals for 22 major acanthomorph clades, as reported in the following 3 phylogenomic studies: Alfaro *et al.*[7], Hughes *et al.*[18] and this study. Estimates for this study are the raw node heights reported in the 1,084-taxa time tree represented in Figs. 1 and 2. The 95% HPD credible interval of stem ages for most of the represented clades overlap with previous estimates, but we observe some major discrepancies, likely due to differences in tree topologies and taxon sampling. Fish illustrations by Julie Johnson.

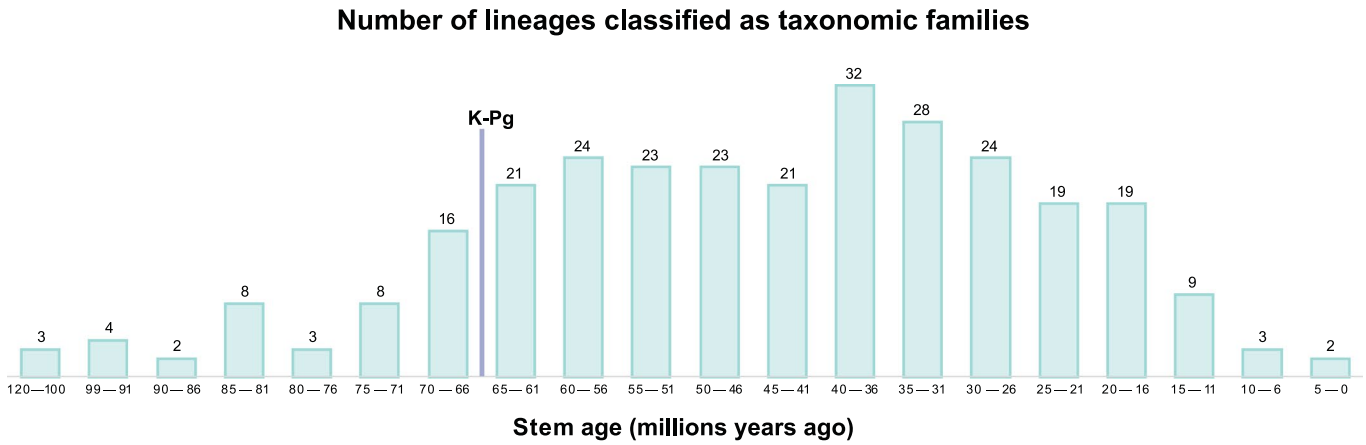

Extended Data Fig. 4 | Acanthomorph lineages classified as taxonomic families underwent a steady period of increased origination beginning at the K-Pg boundary. Bar plot of the estimated number of lineages classified as taxonomic families originating during 5 million year bins. Note that the amounts of time represented by the first two bars are greater than the 5 million years represented by all other bars.

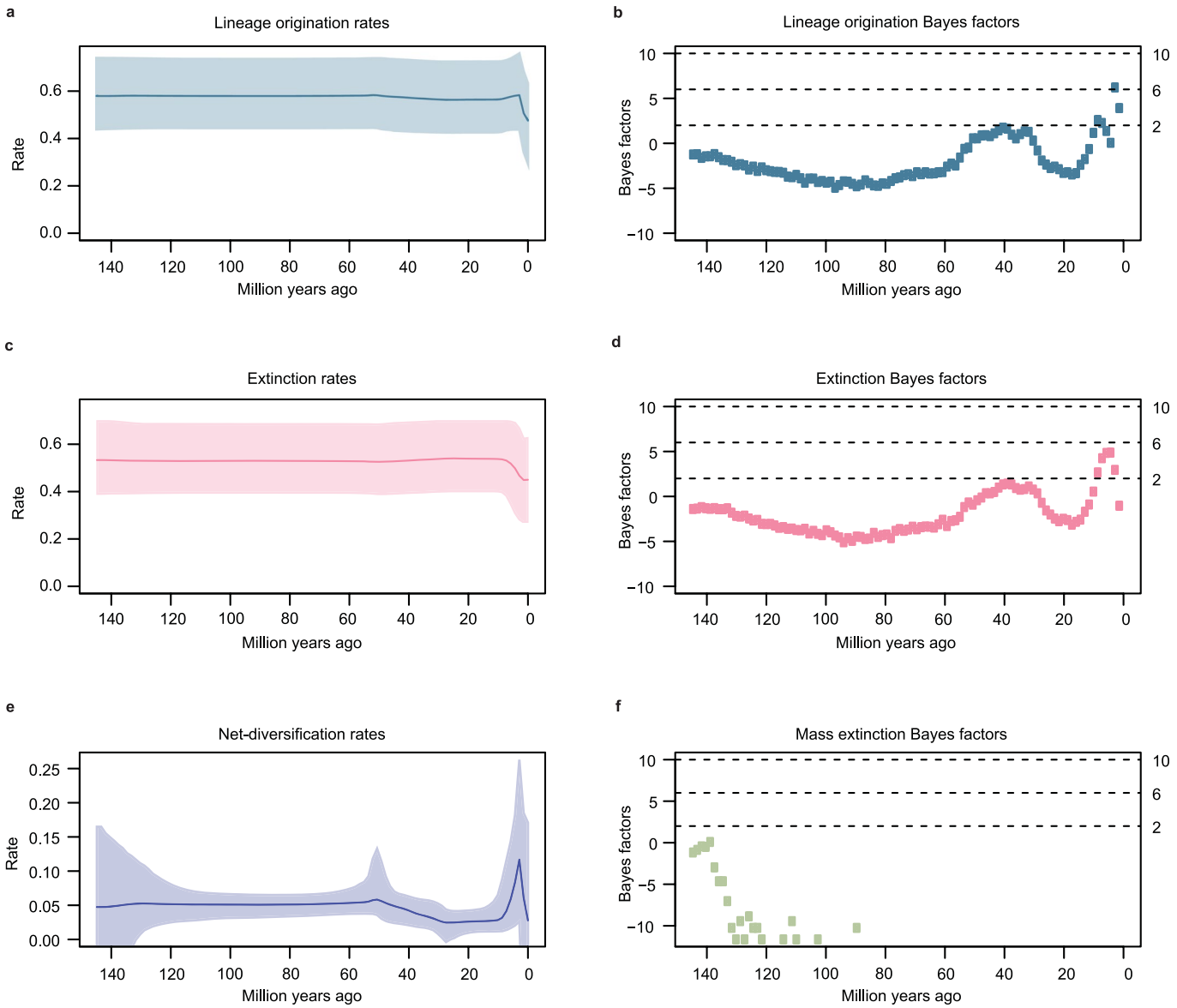

Extended Data Fig. 5 | TESS-CoMET analyses suggest constant tree-wide diversification rates through most of the history of Acanthomorpha. In **b**, **d**, and **e**, horizontal dashed lines and the right-hand y-axis mark statistical support cutoffs for rate shifts, with $2 \leq$ Bayes factors (BF) < 6 considered to be low support, $6 \leq$ BF < 10 considered to be moderate support and ≥ 10 considered to be high support. The rate shifts observed in **a**, **c**, and **e** over the last 10 million years are likely an artifact of the CoMET model (see **Supplementary Information** for further discussion). **a**, Posterior mean (blue line) and 95% credible interval (blue shading) for acanthomorph lineage origination (that is speciation) rates through time. **b**, Bayes factor (BF) support for a shift in lineage origination rate at every 1 Myr time period. **c**, Posterior mean (pink line) and 95% credible interval (pink shading) for acanthomorph lineage extinction rates through time. **d**, Bayesian support (in BF) for a shift in extinction rate at every 1 Myr time period. **e**, Posterior mean (violet line) and 95% credible interval (violet shading) for acanthomorph net-diversification (origination minus extinction) rates through time. Though this plot suggests that there is a small shift in net-diversification rate ~50 Mya, there is no statistical support for such a shift (see **b** and **d**). **f**, There is no statistical support (in BF) for a mass extinction event in Acanthomorpha at any 1 Myr time period.

Model 1 (Null)	Model 2 (Alternative)	2ln(BF)
Constant BD Uniform Sampling	Mass Extinction BD Diversified Sampling	55,487.1
Episodic BD (shift at 50 mya) Uniform Sampling	Mass Extinction BD Diversified Sampling	55,480.7
Decreasing Speciation Rate BD Uniform Sampling	Mass Extinction BD Diversified Sampling	55,477.2
Episodic BD (shift at 50 mya) Diversified Sampling	Mass Extinction BD Diversified Sampling	54,609.6
Decreasing Speciation Rate BD Diversified Sampling	Mass Extinction BD Diversified Sampling	50,634.5
Constant BD Diversified Sampling	Mass Extinction BD Diversified Sampling	49,838.1
Constant BD Uniform Sampling	Mass Extinction BD Uniform Sampling	29,863.0
Episodic BD (shift at 50 mya) Uniform Sampling	Mass Extinction BD Uniform Sampling	29,856.6
Decreasing Speciation Rate BD Uniform Sampling	Mass Extinction BD Uniform Sampling	29,853.1
Episodic BD (shift at 50 mya) Diversified Sampling	Mass Extinction BD Uniform Sampling	28,985.5
Mass Extinction BD Uniform Sampling	Mass Extinction BD Diversified Sampling	25,624.1
Decreasing Speciation Rate BD Diversified Sampling	Mass Extinction BD Uniform Sampling	25,010.4
Constant BD Diversified Sampling	Mass Extinction BD Uniform Sampling	24,214.0
Constant BD Uniform Sampling	Constant BD Diversified Sampling	5,649.0
Episodic BD (shift at 50 mya) Uniform Sampling	Constant BD Diversified Sampling	5,642.6
Decreasing Speciation Rate BD Uniform	Constant BD Diversified Sampling	5,639.1
Constant BD Uniform Sampling	Decreasing Speciation Rate BD Diversified Sampling	4,852.6
Episodic BD (shift at 50 mya) Uniform Sampling	Decreasing Speciation Rate BD Diversified Sampling	4,846.2
Decreasing Speciation Rate BD Uniform Sampling	Decreasing Speciation Rate BD Diversified Sampling	4,842.7
Episodic BD (shift at 50 mya) Diversified Sampling	Constant BD Diversified Sampling	4,771.5
Episodic BD (shift at 50 mya) Diversified Sampling	Decreasing Speciation Rate BD Diversified Sampling	3,975.1
Constant BD Uniform Sampling	Episodic BD (shift at 50 mya) Diversified Sampling	877.5
Episodic BD (shift at 50 mya) Uniform Sampling	Episodic BD (shift at 50 mya) Diversified Sampling	871.1
Decreasing Speciation Rate BD Uniform Sampling	Episodic BD (shift at 50 mya) Diversified Sampling	867.6
Decreasing Speciation Rate BD Diversified Sampling	Constant BD Diversified Sampling	796.4
Constant BD Uniform Sampling	Decreasing Speciation Rate BD Uniform Sampling	9.9
Constant BD Uniform Sampling	Episodic BD (shift at 50 mya) Uniform Sampling	6.4
Episodic BD (shift at 50 mya) Uniform Sampling	Decreasing Speciation Rate BD Uniform Sampling	3.5

Extended Data Fig. 6 | See next page for caption.

Extended Data Fig. 6 | Pairwise comparisons of 8 birth-death (BD) branching process models. TESS calculated Bayes Factors (2ln(BF)) from the pairwise comparisons of marginal likelihoods for 8 birth-death (BD) branching-process models with the following priors: 1.) constant diversification rate with uniform (random) sampling, 2.) constant diversification rate with diversified sampling (sampling results in even coverage of all clades), 3.) decreasing speciation rate with uniform sampling, 4.) decreasing speciation rate with diversified sampling, 5.) constant diversification rate with a rate shift 50 Mya ('Episodic BD') with uniform sampling, 6.) constant diversification rate with a rate shift 50 Mya ('Episodic BD') with diversified sampling, 7.) constant speciation rate with a single mass extinction event occurring at any point in time ('Mass Extinction BD') with uniform sampling, and 8.) constant speciation rate with a single mass extinction event occurring at any point in time ('Mass Extinction BD') with diversified sampling. Observations of the pairwise comparisons note strong preference for a model that assumes uniform (random) sampling and strong support for either a constant rate BD model, or an episodic BD model that assumes a shift 50 mya. There is moderate Bayesian support (2ln(BF) = 6.4) that among the models assuming uniform sampling, the constant rate model is preferred over the model with a shift 50 Mya.

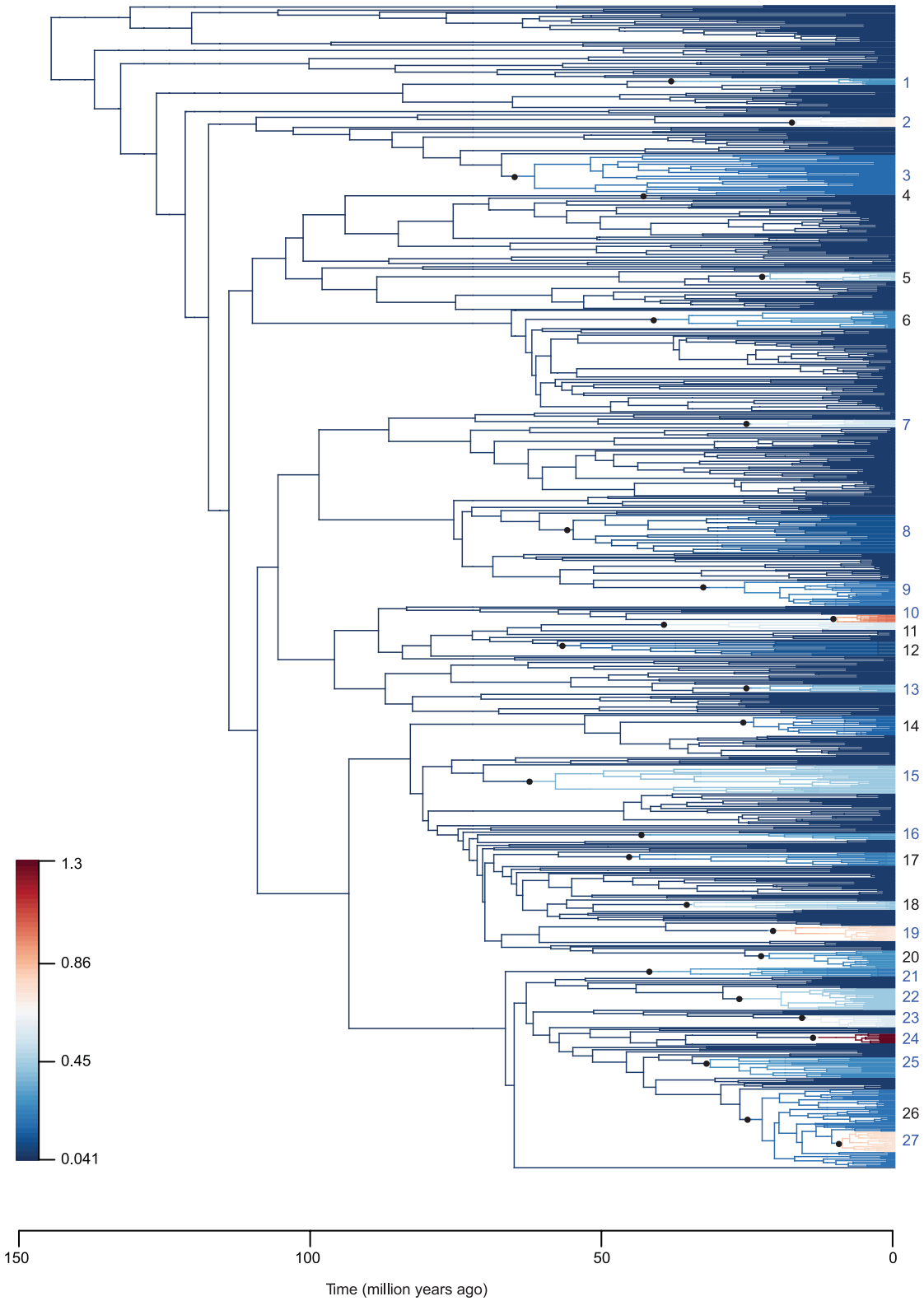

Extended Data Fig. 7 | See next page for caption.

Extended Data Fig. 7 | Visual summary of shifts in speciation rates inferred using BAMM. The configuration presented here is the maximum shift credibility (MSC) configuration for an analysis that expected 15 rate shifts under the prior. Darker red colors depict relatively fast rates, while darker blue colors depict relatively slow rates. Rate shifts along branches are denoted with filled, black circles and assigned identifying numbers. Shifts in speciation rate are estimated to have occurred on the branches leading to the following 27 clades: 1.) Dinematichthyidae, 2.) Apogonidae (to the exclusion of *Pseudamia*), 3.) Gobiidae and Oxudercidae, 4.) *Solenostomus*, 5.) *Parupeneus* and *Pseudopeneus* (in Mullidae), 6.) *Ariomma*, Nomeidae and Stromateidae, 7.) Mastacembelidae, 8.) the clade defined by Scophthalmidae and Soleidae, 9.) Carangidae (to the exclusion of *Seriola*), 10.) Pseudocrenilabrinae (in Cichlidae), 11.) Pomacentridae, 12.) the clade defined by Gobiesocidae and Dactyloscopidae, 13.) Poeciliidae, 14.) the clade defined by Scorpididae and Terapontidae, 15.) Labridae, 16.) Sciaenidae, 17.) the clade defined by Nemipteridae and Sparidae, 18.) Tetraodontidae, 19.) Chaetodontidae, 20.) Acanthuridae (to the exclusion of *Prionurus* and *Naso*), 21.) Anthiadinae and Epinephelidae, 22.) darters (Etheostomatinae), 23.) the clade defined by Nototheniidae and Channichthyidae, 24.) *Sebastes*, 25.) the clade defined by Trichodontidae and Psychrolutidae, 26.) the clade defined by Stichaeidae and Zoarcidae and 27.) the clade defined by *Bothrocara* and *Lycodes concolor* (in Zoarcidae). Shifts labelled with blue rather than black numbers are estimated to have occurred by 16 of the 23 BAMM analyses conducted in this study. Although shift number 20 and shift number 26 are labelled in black, the vast majority of BAMM analyses predicted a rate shift in nearby branches leading to slightly more inclusive clades (specifically Acanthuridae to the exclusion of *Naso*, and all of Lycodinae, respectively).

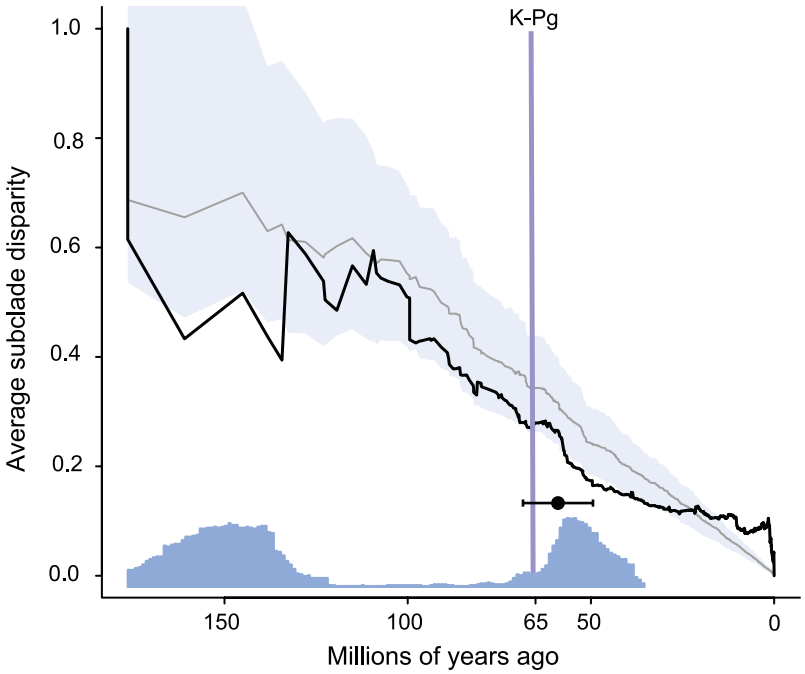

Extended Data Fig. 8 | Mean relative disparity through time (DTT) for all of Acanthomorpha, calculated using the combined data for seven phenotypic measurements and repeated on a sample of 100 trees from the posterior distribution of time-trees. The gray line and blue shaded region indicate the median and 95% confidence interval (CI) expected under a Brownian motion model (BM) of evolution, respectively, and the solid black line indicates the observed pattern of disparity. This is the same plot visualized in Fig. 2, but note that the earliest portion of the DTT plot that includes the outgroup is not shown in Fig. 2. Acanthomorph body shapes radiated for approximately 15–20 million years in the aftermath of the K-Pg, followed by within-lineage phenotypic diversification. The blue histogram along the x-axis shows the proportion of time-calibrated trees for which the null hypothesis is rejected ($P < 0.05$) and the observed disparity falls outside of the BM model's 95% CI in each one-million-year interval. The inset, black box-and-whisker plot depicts the mean (±95% CI) of the initial time point at which the observed disparity dropped below that expected from BM following the K-Pg.

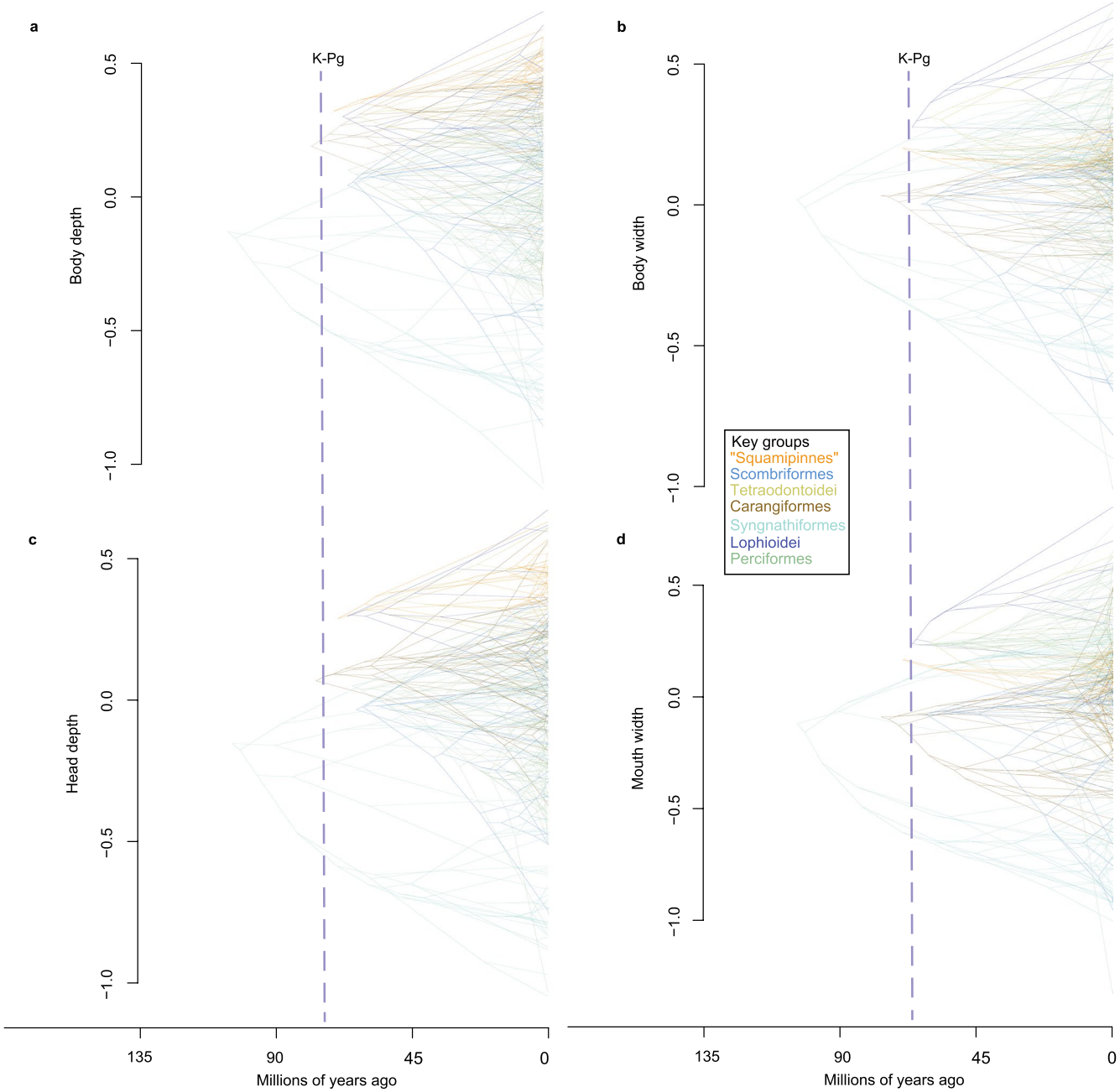

Extended Data Fig. 9 | Phenograms depicting the evolutionary history of four size-corrected phenotypic traits (body depth and width, head depth, and mouth width) across seven major lineages that arose around the K-Pg. The vertical dashed line marks the K-Pg boundary. Note that not all major acanthomorph lineages are represented in these plots and that Lophioidei and Tetraodontoidei are major subclades of Acanthuriformes. 'Squamipinnes' refers to the acanthuriform clade in Supplementary Fig. 23 defined by *Chaetodon kleinii* and *Luvarus imperialis*.

nature portfolio

Corresponding author(s): Ava Ghezelayagh

Last updated by author(s): Apr 1, 2022

Reporting Summary

Nature Portfolio wishes to improve the reproducibility of the work that we publish. This form provides structure for consistency and transparency in reporting. For further information on Nature Portfolio policies, see our Editorial Policies and the Editorial Policy Checklist.

Statistics

For all statistical analyses, confirm that the following items are present in the figure legend, table legend, main text, or Methods section.

n/a	Confirmed
☐	☒ The exact sample size (*n*) for each experimental group/condition, given as a discrete number and unit of measurement
☐	☒ A statement on whether measurements were taken from distinct samples or whether the same sample was measured repeatedly
☒	☐ The statistical test(s) used AND whether they are one- or two-sided *Only common tests should be described solely by name; describe more complex techniques in the Methods section.*
☐	☒ A description of all covariates tested
☐	☒ A description of any assumptions or corrections, such as tests of normality and adjustment for multiple comparisons
☐	☒ A full description of the statistical parameters including central tendency (e.g. means) or other basic estimates (e.g. regression coefficient) AND variation (e.g. standard deviation) or associated estimates of uncertainty (e.g. confidence intervals)
☒	☐ For null hypothesis testing, the test statistic (e.g. *F*, *t*, *r*) with confidence intervals, effect sizes, degrees of freedom and *P* value noted *Give P values as exact values whenever suitable.*
☐	☒ For Bayesian analysis, information on the choice of priors and Markov chain Monte Carlo settings
☒	☐ For hierarchical and complex designs, identification of the appropriate level for tests and full reporting of outcomes
☐	☒ Estimates of effect sizes (e.g. Cohen's *d*, Pearson's *r*), indicating how they were calculated

Our web collection on statistics for biologists contains articles on many of the points above.

Software and code

Policy information about availability of computer code

Data collection	Whole genomic DNA was downloaded from NCBI and converted to 2bit format using faToTwoBit from the UCSC Genome Browser Downloads (https://hgdownload.cse.ucsc.edu/admin/exe/). UCE loci were located from each genome assembly using the publicly available PHYLUCE v.1.7.1 script run_multiple_lastzs_sqlite.py with default parameters and the FASTA file containing the UCE bait sequences. The program phyluce_probe_slice_sequence_from_genomes.py was used (with default parameters) to extract the identified loci.
Data analysis	No custom code needed for reproducibility, but the following open source programs were used for data analysis: the pipeline PHYLUCE v.1.7.1, MAFFT v7.130b, trimAL v1.4.rev, IQTREE v.1.7, IQTREE v.2, PartitionFinder2 v2.1.1, RAxML-ng v0.9.0, TOPD_v4.6, BEAST v.1.8.4 , BEAST v2.5, ASTRAL-III v5.6.3, BUCKy, BAMM v.2.5.0, and the following R packages: TESS, PHYTOOLS, GEIGER. Citations to all software used are given in the manuscript. Code availability Analyses relied on open source programs and scripts used for data analysis are available on the Dryad Digital Repository: https://datadryad.org/stash/share/-vfd5XqnNuJ1BHG7s2nBDw2nRRyK80Rc4BAtkrAkkoU . Data availability NCBI BioSample Accession numbers corresponding to sequence data are listed in Supplementary Table 1. New raw sequence data is available for download from the NCBI Sequence Read Archive (SRA), under BioProject ID PRJNA758064. Sequence alignments, partitioning schemes, phylogenetic trees, and other related data files are available on the corresponding Dryad Digital Repository: https://datadryad.org/stash/share/-vfd5XqnNuJ1BHG7s2nBDw2nRRyK80Rc4BAtkrAkkoU.

For manuscripts utilizing custom algorithms or software that are central to the research but not yet described in published literature, software must be made available to editors and reviewers. We strongly encourage code deposition in a community repository (e.g. GitHub). See the Nature Portfolio guidelines for submitting code & software for further information.

Data

Policy information about availability of data

All manuscripts must include a data availability statement. This statement should provide the following information, where applicable:

- Accession codes, unique identifiers, or web links for publicly available datasets
- A description of any restrictions on data availability
- For clinical datasets or third party data, please ensure that the statement adheres to our policy

Data availability
NCBI BioSample Accession numbers corresponding to sequence data are listed in Supplementary Table 1. New raw sequence data is available for download from the NCBI Sequence Read Archive (SRA), under BioProject ID PRJNA758064. Sequence alignments, partitioning schemes, phylogenetic trees, phenotypic trait data, and other related data files are available on the corresponding Dryad Digital Repository: https://datadryad.org/stash/share/-vfd5XqnNuJ1BHG7s2nBDw2nRRyK80Rc4BAtkrAkkoU.

Field-specific reporting

Please select the one below that is the best fit for your research. If you are not sure, read the appropriate sections before making your selection.

☐ Life sciences ☐ Behavioural & social sciences ☒ Ecological, evolutionary & environmental sciences

For a reference copy of the document with all sections, see nature.com/documents/nr-reporting-summary-flat.pdf

Ecological, evolutionary & environmental sciences study design

All studies must disclose on these points even when the disclosure is negative.

Study description	A phylogenetic analysis of 1,084 species of teleosts fishes (1,109 individual specimens; duplicates for species are noted in Supplementary Table 1). The phylogeny is time-calibrated using information from the fossil record. The pattern of body shape diversification from 608 teleost species (one individual per species) is explored using the phylogeny.
Research sample	We include genomic data sampled from 1,084 species of teleost fishes targeting 91% of the taxonomic families. The taxon sampling, which used museum accessions of fish tissues, was designed to capture the major lineages of acanthomorph fishes. Some of the species were already sequenced (e.g. Alfaro et al. (2018)) and we gathered the appropriate data from NCBI.
Sampling strategy	We were interested in relationships among major lineages, so we typically only included one specimen per species sampled.
Data collection	All new DNA sequencing was performed by Ava Ghezelayagh, Peter Cowman, Richard Harrington, and Jessica Glass.
Timing and spatial scale	All new DNA sequence data was collected in 2018 and 2019.
Data exclusions	No sequence data was excluded. For diversification rate analyses, trees were pruned to exclude outgroup and duplicate that would be irrelevant to the question and/or drive misleading results.
Reproducibility	Some species were sequenced with multiple individuals to test the veracity of our data work flow. These duplicates can be found in Supplementary Table 1. We report all protocols for the generation of phylogenomic data in the Methods section of the Supplementary Information, allowing for the reproduction of alignments and downstream phylogenetic analyses using open source, previously published code.
Randomization	This is not particularly relevant to phylogenetic analyses concerning historical evolution. The only relevant randomization that occurred was the random selection of time trees outputted by BEAST to produce a summary Maximum Clade Credibility tree with TreeAnnotator. This randomization was performed using the shuf command in Unix.
Blinding	This is not relevant to phylogenetics.

Did the study involve field work? ☐ Yes ☒ No

Reporting for specific materials, systems and methods

We require information from authors about some types of materials, experimental systems and methods used in many studies. Here, indicate whether each material, system or method listed is relevant to your study. If you are not sure if a list item applies to your research, read the appropriate section before selecting a response.

Materials & experimental systems

n/a	Involved in the study
☒	☐ Antibodies
☒	☐ Eukaryotic cell lines
☒	☐ Palaeontology and archaeology
☐	☒ Animals and other organisms
☒	☐ Human research participants
☒	☐ Clinical data
☒	☐ Dual use research of concern

Methods

n/a	Involved in the study
☒	☐ ChIP-seq
☒	☐ Flow cytometry
☒	☐ MRI-based neuroimaging

Animals and other organisms

Policy information about studies involving animals; ARRIVE guidelines recommended for reporting animal research

Laboratory animals	NA
Wild animals	NA
Field-collected samples	Tissue samples of animals used in this study were obtained from several research museum collections, listed in the Acknowledgments.
Ethics oversight	The Peabody Museum of Natural History is under the ethics mandate of IACUC, so any tissues used from the Peabody collection followed IACUC approval. However, no animal or paleontological materials were collected for the purpose of this study and the study itself did not require IACUC approval.

Note that full information on the approval of the study protocol must also be provided in the manuscript.